Semi-Inclusive Deep Inelastic Scattering Measurements of $A = 3$ Nuclei with CLAS12 in Hall B

S. Li, R. Cruz Torres, J. Rittenhouse West (spokesperson), F. Yuan
Lawrence Berkeley National Laboratory, Berkeley, CA 94720, USA

A. Denniston, O. Hen (spokesperson), J. Kahlbow, T. Kutz
J. R. Pybus, E.P. Segarra,
Massachusetts Institute of Technology, Cambridge, Massachusetts 02139, USA

C. Ayerbe-Gayoso, H. Bhatt, D. Bhetuwal, T. Chetry, B. Devkota, J. Dunne,
D. Dutta (spokesperson), L. El Fassi, T. Gaballah, A. Karki,
Mississippi State University, Mississippi State, MS 39762 USA

M. Amarian, C. Fogler, F. Hauenstein, C. Hyde, G. Gavalian,
L.B. Weinstein (spokesperson, contact)
Old Dominion University, Norfolk, Virginia 23529, USA

D. Gaskell (spokesperson), D.W. Higinbotham, C. Keith, C. Keppel,
J. Maxwell, A.Tadepalli, D. Meekins (spokesperson),
D. Nguyen (spokesperson), S. Stepanyan, H. Szumila-Vance
Thomas Jefferson National Accelerator Facility,
Newport News, Virginia 23606, USA

Z.G. Xiao, Y. Wang, Z.H. Ye (spokesperson), Y.P. Zhang
Tsinghua University, Beijing 100084, China

K. Griffioen, P. Bosted
College of William and Mary, Williamsburg, VA 23185, USA

A. Bianconi, G. Costantini, M, Leali, S. Migliorati, L. Venturelli
Dipartimento di Ingegneria dell'Informazione, Università di Brescia, Italy,
and, INFN, sezione di Pavia, Italy

V. Mascagna
DiSAT, Università dell'Insubria, Como, Italy,
and, INFN, sezione di Pavia, Italy

A. Boyer, F. Benmokhtar, A. Gadsby, A. Parker
Duquesne University, Pittsburgh, PA 152028 USA

L. Baashen, B. Raue
Florida International University, Miami, FL 33199 USA

W. J. Briscoe, S. Ratliff, A. Schmidt, E. Seroka, P. Sharp, P. G. Solazzo,
I. I. Strakovsky
The George Washington University, Washington DC 20052, USA

K. Adhikari
Hampton University, Hampton, VA 23669, USA

G. Niculescu,
James Madison University, Harrisonburg, VA 22807, USA

K.-T. Brinkmann, S. Diehl, A. Kripko
Justus Liebig University Giessen, 35390 Giessen, Germany

Sheren Alsalmi
King Saud Univeristy, Riyadh, Saudi Arabia

Tyler J Hague
North Carolina Agricultural and Technical State University, NC, USA

A. Beck, S. Beck, E. CohenI. Korover
Nuclear Research Center Negev, Be'er Sheva, Israel

G. Johansson, C. Neuburger, E. Piasetzky
Tel-Aviv University, Tel Aviv 69978, Israel

Michael Nycz
Temple University, Philadelphia, PA 19122, USA

R. Capobianco, T. Haywars, F.-X. Girod, K. Joo, A. Kim, V. Klimenko,
R. Santos, U. Shrestha, P. Simmerling, J. Richard, N. Trotta,
University of Connecticut, Storrs, CT, USA

B. McKinnon
University of Glasgow, Glasgow, United Kingdom

W. Brooks
Universidad Técnica Federico Santa María, Valparaíso, Chile

And the CLAS Collaboration

May 24, 2021

Abstract

We propose to measure precision ratios of charged pion electroproduction in Semi-Inclusive Deep Inelastic Scattering from ^{2}D, ^{3}He and ^{3}H targets to test the flavor dependence of the EMC effect in the valence quark region. This trio of targets has been chosen to minimize hadron attenuation effects while maximizing nuclear asymmetry. The standard configuration CLAS12 detector will be used in the experiment to detect scattered electrons and knocked-out pions. A new, dedicated, tritium target that will be developed for the approved quasi-elastic experiment, E12-20-005 [1], will be used. The experiment will measure semi-inclusive production of charged pions over a wide range of Bjorken-x variable. It will focus on $z = E_\pi/\nu \geq 0.3$ to maximize the connection between the struck quark and the detected $\pi^\pm$. Double ratios of the total yields and ratios of the yield differences between $A = 3$ nuclei to ^{2}D will be formed in order to search for evidence of a flavor dependence in the EMC effect, giving us new data on the effect of the nuclear environment on quarks. Our simulations show that these double ratio variables are most sensitive to potential flavor dependence of the EMC effects. Double ratios between the $A = 3$ mirror nuclei can also provide a direct measurement of the d/u ratios at large x thanks to their similar and well understood nuclear corrections. While there is a dearth of calculations of flavor dependence for $A = 3$ nuclei, we expect our data will stimulate a surge of new calculations. In addition to ratios, we will also measure $(e, e'\pi^+)$ and $(e, e'\pi^-)$ cross sections as a function of x, Q^2, z, P_T to allow theorists to extract the unpolarized TMDs, PDFs and fragmentation functions in $A = 3$ nuclei. If the CLAS12 RICH is available we will also measure flavor-tagged DIS with kaons. This proposal builds on PR12-09-004, a proposal to observe the ratio of gold to deuterium that was determined to have too many nuclear uncertainties. By using ratios of light nuclei, we maintain the sensitivity to the underlying physics but dramatically decrease the nuclear uncertainties due to attenuation and hadronization in heavy nuclei. This experiment is very timely because it will extend the newly published inclusive MARATHON studies of ^{3}H and ^{3}He to the semi-exclusive regime by flavor-tagging the struck quarks.

1 Introduction

One of the longstanding goals of nuclear physics is to understand how nuclei can be described in terms of the color charge carrying quarks and gluons of the fundamental theory of the strong force – Quantum Chromodynamics (QCD). An exploration and confirmation of QCD as the ultimate source of the strong interaction requires exploring the true nature of color confinement in the nuclear environment [2, 3]. Nuclei provide an excellent testing ground for QCD because they are stable systems made of quarks and gluons bound together by the strong force. However, quarks and gluons in nuclei are hidden by the confining nature of QCD. Effective theories of nucleons exchanging mesons as the effective degrees of freedom describe nuclear dynamics quite well, but a deeper investigation is needed to probe quark and gluon dynamics. Over the last several decades a significant amount of effort has been invested in the study of nuclear structure at small distances to map out the quark distributions inside nuclei and find novel signatures of QCD in nuclei.

The discovery in 1983 of an unexpected depletion of the per-nucleon deep inelastic scattering (DIS) cross-section (or, equivalently, nuclear structure function F_2) in a nucleus as compared to that in a free nucleon [4] (see Fig. 1) was dubbed the "EMC effect" and was the first major evidence of quark effects in nuclei. It demonstrated that nuclei cannot be described simply as collections of nucleons. Following its original observation by the EMC collaboration, the modification of structure functions in nuclei has created a cottage industry of theoretical and experimental efforts aimed at understanding its origin (see [5–8] for reviews). For example, the A and x dependence of the EMC effect has been precisely mapped out using inclusive DIS studies by the SLAC E139 experiment [9], while the nuclear density dependence for low mass nuclei has been precisely measured at JLab [10] revealing a possible local density dependence of the EMC effect. A multitude of theoretical approaches, ranging from nuclear binding and convolution models to dynamical quark rescaling, as well as quark-meson coupling inspired approaches [11] are all able to describe the EMC effect quite

adequately in the high x regime. Yet, to date, there is no generally accepted explanation of the EMC effect and its specific origin has not been unambiguously identified.

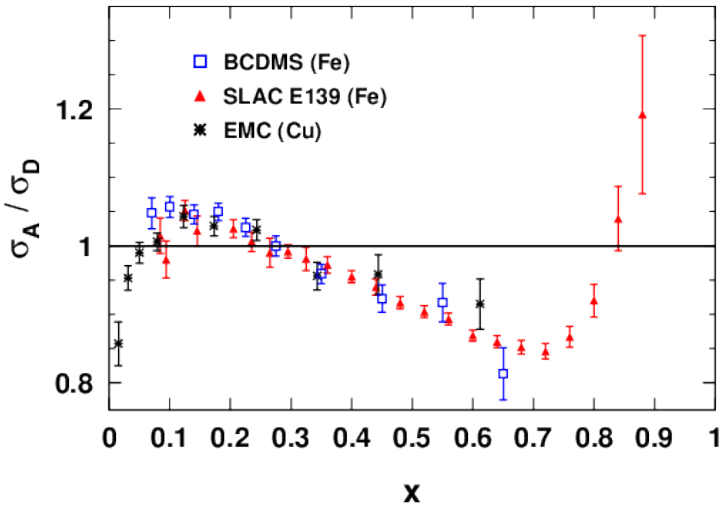

Figure 1: Cross section ratios from copper and iron to deuterium from the EMC [4], BCDMS [12] and SLACE139 [9] experiments.

Almost all previous EMC measurements have been inclusive and do not provide sufficient insight into the QCD mechanism behind the modification of the nuclear structure functions. The measurements at large x are measurements of the same observable, i.e. σ_A/σ_D, with additional constraints from measurements of the A-dependence of the sea quark distribution in Drell-Yan reactions [13]. Therefore, we know that the EMC effect requires some level of nucleon-structure modification in nuclei, but there is no generally accepted description. We need new experimental observables to better understand the QCD dynamics of multi-nucleon systems at small distances, thereby unraveling the mystery of the EMC effect.

An intriguing similarity between the nuclear dependence of high-momentum nucleons or short-range correlations (SRC) and the nuclear dependence of the EMC effect has been observed [8,14–16]. This correlation between the number of SRC pairs and the size of the EMC effect suggests the possibility of a close connection between these two effects. There are two leading hypotheses to account for this correlation. First, that the EMC effect is directly sensitive to the contribution of SRCs because the EMC effect is a result of high-momentum nucleons and can be described by a universal modification of the structure of nucleons in np SRC pairs [17]. Second, that the EMC effect is driven by the presence of super-dense fluctuations in nuclei when two or more nucleons overlap, and thus the EMC-SRC correlation exists because both phenomena are driven by short distance configurations [18]. The experimentally well documented np dominance of SRC pairs [19–22] implies that if the EMC effect is driven by high-momentum nucleons, the fractional contributions from high-momentum protons and neutrons would be different in asymmetric nuclei ($N \neq Z$) giving rise to an isospin (flavor) dependence to the modification of quark distributions in nuclei. On the other hand, if the EMC effect is due to super-dense fluctuations in nuclei, it could be isospin independent if all short-distance pairs (nn, pp, and np) contributed equally [23]. The first hypothesis is strongly preferred by a theoretical study using ab-initio calculations, which found that nucleons at short-range and in high-momentum correlations are the same [24]. New theoretical studies of diquark degrees of freedom in $A = 3$ [25] and $A = 4$ [26] nuclei predict isospin-dependent SRCs and require

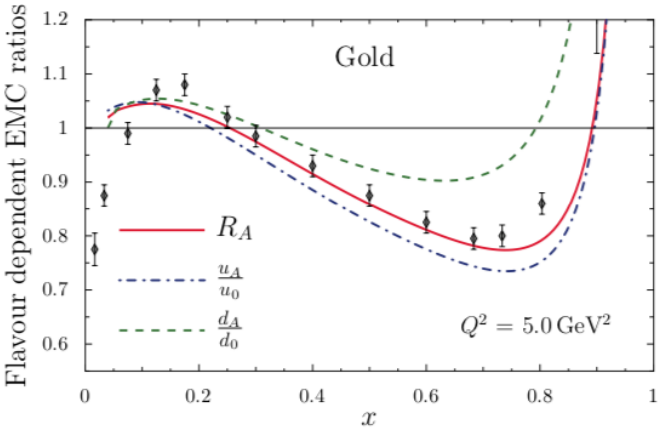

Figure 2: Calculation of the EMC Effect in gold from [29]. Here, "gold" refers to a calculation for nuclear matter, but assuming the same N/Z as gold. In this model, nuclear quark distributions are modified via interactions with vector and scalar fields in the nucleus. The solid red curve shows the overall modification of the nuclear structure function, F_2. The isospin dependence of the interaction generates a different degree of modification for the up and down quark distributions (shown by the green and blue curves respectively). Nuclear matter "data" points are from [33].

precise flavor dependent experimental data to confirm or rule out. Additional data, preferably with newer and more sensitive techniques, are needed to study the flavor dependence of the EMC effect. Unambiguous knowledge of the flavor dependence would provide insight into the origin of the EMC effect and its connection to SRCs. Moreover, it has potential consequences for the NuTev anomaly in neutrino scattering and charge symmetry violation in quark distributions inside nucleons [27–29].

The correlation of the size of the EMC effect with the number of SRC pairs and their *np* dominance is not the only reason to expect flavor dependence in the EMC effect. Many simple descriptions of the EMC effect naturally produce larger effects in protons compared to neutrons in asymmetric nuclei [7, 29]. Calculations using the quark-meson coupling (QMC) model [30] for "gold" (i.e., for nuclear matter using the same N/Z as gold) predict that the up quark distribution is significantly more modified than the down quark distribution (see Fig. 2). A recent calculation which incorporates a QCD color-singlet configuration in nuclei via a strongly bound combination of six scalar isospin-0 [*ud*] diquarks within the nuclear wave function also predicts an isospin dependent ("iso-phobic") EMC effect [26]. Moreover, the first indication of an iso-vector EMC effect was recently reported by combining the ^{3}He/^{3}H data from the MARATHON experiment [31] with a global QCD analysis to simultaneously extract PDFs and nuclear effects in $A = 2$ and $A = 3$ nuclei [32]. Therefore, the flavor dependence of the EMC effect is one of the most promising new avenues for precision studies of the EMC effect and it is critical to developing experimental techniques that are sensitive to it.

One such promising experimental technique is the semi-inclusive $(e, e'\pi^{\pm})$ DIS (SIDIS) reaction. Semi–inclusive DIS can be used as a "flavor tag" (see Fig. 3) to look for signatures of differences in the EMC effect in the up and down quark distributions in mirror nuclei. It has been used successfully, most notably by the HERMES collaboration [34], to deconvolute the relative contributions of up, down, and sea quarks to the spin of the nucleon. However, one can just as easily employ the power of this technique to probe the unpolarized degrees of freedom rather than polarized parton distributions.

SIDIS measurements on mirror nuclei is one of the most effective ways to enhance the sensitivity of this technique, while simultaneously reducing the impact of hadron attenuation. For example, if the EMC effect is due to the modification of the structure functions of nucleons in *np* SRC pairs,

the single proton in ^{3}H can belong to one of two np SRC pairs, but the two neutrons in ^{3}H can each belong to only one. Therefore, the proton in ^{3}H will be more modified than the average of the neutrons. This effect will be reversed in ^{3}He, where the neutron will be more modified than the average of the protons. A clear demonstration of the power of the data from mirror nuclei comes from the recent spate of articles [35] stimulated by the MARATHON results [32], such as the one reporting the first indication of an iso-vector EMC effect.

However, currently there are no definitive predictions of the flavor dependence in A=3 nuclei. This absence means we need a data-driven search for the flavor dependence of the EMC effect. These new experimental data should then stimulate a surge of new calculations.

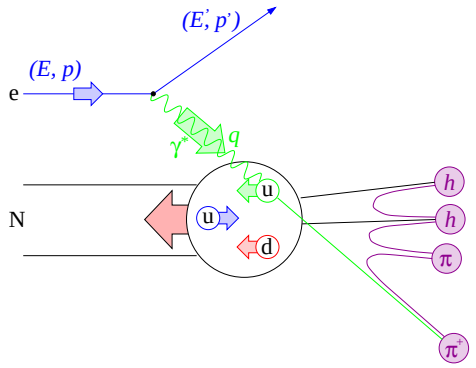

Figure 3: Diagram of semi-inclusive pion production from the nucleon (proton in this diagram). In this picture, the observed hadron (here the π^+) serves as a "tag" of the flavor of the struck (up) quark.

The SIDIS measurement on $A = 3$ mirror nuclei will also provide direct access (at leading order) to the nucleon d/u ratio at high x as $x \to 1$. This will help fill the gap in our knowledge of the PDFs as $x \to 1$, in particular the d-quark distributions, arising from the lack of free neutron targets. The SIDIS measurement will be free of most of the theoretical corrections and associated uncertainties that are used to account for the bound neutron in DIS from light nuclei. Moreover, with its entirely different systematics, the SIDIS measurement will be complementary to the recent DIS measurements by MARATHON [36] and the spectator tagged measurements by BoNuS12 [37], BAND and LAD experiments [38]. Moreover, comparing the d/u ratio extracted from the A=3 nuclei to those extracted from deuterium by the BoNuS12 experiment may provide unique insight into the EMC effect.

The SIDIS measurement on $A = 3$ nuclei will also provide the first high precision determination of the fragmentation functions (FF) and unpolarized transverse momentum dependent distributions (TMD), which are important for establishing the 3D structure of nucleons, a major priority for a complete QCD based understanding of the nucleon. When compared to the FF and TMD obtained from Deuterium they will also provide unique information on the nuclear modification of these distributions and hence of the EMC effect.

We propose to study the flavor dependence of the EMC effect at large x using a new observable, the ratio of charged pion electroproduction in semi-inclusive DIS from deuterium, ^{3}He and ^{3}H targets. The new observables proposed here are the super-ratio of the sum in yields $Y(\pi^+) + Y(\pi^-)$ and the ratio of the difference in yields $Y(\pi^+) - Y(\pi^-)$ for the different nuclei. These observables are sensitive to any flavor dependence in modifications to the structure functions inside a nucleus. Thus, by performing a precision measurement of these observables we will expose flavor dependence in the EMC effect and thereby reveal the details of quark dynamics in nuclei which lead to the modification of the nuclear structure functions.

This is primarily a data driven search for such effects, since there is a lack of exact calculations

for A=3 nuclei. However, it will help confirm or refute recent QCD-level theories of the EMC effect [25, 26]. Additionally, these data will also provide unique determinations of the d/u ratio, FF, TMD, and information on factorization and hadron attenuation, as well as spur new theoretical calculations.

2 Physics Goals

We plan to measure the cross-sections of the SIDIS $\pi^{\pm}$ production with unpolarized electrons scattering off unpolarized targets, ^{2}D, ^{3}H and ^{3}He. The wide acceptance of CLAS12 allows us to perform multi-dimensional binning (e.g., x, Q^2, z, P_T) of the SIDIS data with great precision to help disentangle the x- and z-dependencies. These will enable theorists to study with great detail the effects in the different nuclei. We will study the flavor-dependent EMC effect in $A = 3$ nuclei, probe the d/u ratios at high-x by taking advantage of the theoretically well controlled nuclear effects in ^{3}H and ^{3}He , and map out the three-dimensional parton distributions functions and fragmentation functions. The SIDIS data binned in multiple dimensions (e.g., Q^2, x, z, and P_T) also allow us to study the factorization theorem and understand the hadronization process in light nuclei. The planned upgrade of the CLAS12 with a full-size RICH detector would simultaneously provide us the SIDIS kaon-production data for the study of the strangeness content in the $A = 3$ Nuclei, although it is not the major goal of this proposal.

In this section, we adopt the framework of the leading-order approximation. Although simplified,it shows the experimental sensitivities and lets us discuss the physics goals of our proposed measurements. The actual extraction of physics will need full theoretical calculations. The SIDIS cross-section for electrons scattering off an unpolarized proton,can be expressed as:

$$\frac{d\sigma_p^h}{dxdQ^2dz} = \frac{4\pi\alpha^2 s}{Q^4}(1 - y + \frac{y^2}{2})F_{UU}^h(x, z), \tag{1}$$

where,

$$F_{UU}^h(x, z) = \sum_q e_q^2 f_1^q(x) \cdot D_q^h(z), \tag{2}$$

are the unpolarized SIDIS structure functions after integrating the transverse component. The functions $f_1^q(x)$ and $D_q^h(z)$ are the unpolarized parton distribution functions (PDFs), and unpolarized Fragmentation functions (FFs). In the SIDIS reaction with pion-production, the experimental yields normalized by common experimental quantities (e.g. beam charge, target luminosity, detection efficiency, and kinematic cuts) are proportional to the sum of quark-PDFs multiplied by their associated FFs:

$$\begin{aligned} Y_p^{\pi^{\pm}}(x, z) \propto F_{p,UU}^{\pi^{\pm}} &= e_u^2 \cdot u(x) \cdot D_u^{\pi^{\pm}}(z) + e_u^2 \cdot \bar{u}(x) \cdot D_{\bar{d}}^{\pi^{\pm}}(z) \\ &+ e_d^2 \cdot d(x) \cdot D_d^{\pi^{\pm}}(z) + e_d^2 \cdot \bar{d}(x) \cdot D_{\bar{d}}^{\pi^{\pm}}(z) \\ &+ e_s^2 \cdot s(x) \cdot D_s^{\pi^{\pm}}(z) + e_s^2 \cdot \bar{s}(x) \cdot D_{\bar{s}}^{\pi^{\pm}}(z), \end{aligned} \tag{3}$$

where $e_u = 2/3$, $e_d = -1/3$, and $e_s = -1/3$. Due to the strong correlations of the struck quark and the leading hadron in SIDIS, a common approach in the global analysis of the SIDIS data is to simplify the FFs into a set of "favored" and "unfavored" terms to describe the probabilities of u, d, $\bar{u}$ and $\bar{d}$ fragmenting into $\pi^{\pm}$: $D_u^{\pi^+} = D_{\bar{d}}^{\pi^+} = D_d^{\pi^-} = D_{\bar{u}}^{\pi^-} \equiv D^{\text{fav}}$, $D_d^{\pi^+} = D_{\bar{u}}^{\pi^+} = D_u^{\pi^-} = D_{\bar{d}}^{\pi^-} \equiv D^{\text{unfav}}$, and $D_s^{\pi^{\pm}} = D_{\bar{s}}^{\pi^{\pm}} = D_s$.

In a nucleus with Z protons and N neutrons, we define the nuclear PDF (nPDF) per nucleon as:

$$f_A(x) = \frac{Z\tilde{f}_{p,A} + N\tilde{f}_{n,A}}{A}, \tag{4}$$

where $\tilde{f}_{p,A}$ is the medium-modified quark-distribution in the proton bound in the nucleus A. Assuming isospin symmetry (e.g. $u_p = d_n = u$, $u_n = d_p$, etc.),

$$u_A = \frac{Z\tilde{u} + N\tilde{d}}{A}, d_A = \frac{Z\tilde{d} + N\tilde{u}}{A}, s_A = s, \tag{5}$$

with analogous expressions for the anti-quarks. With that, we can rewrite the per-nucleon SIDIS yield for a nucleus:

$$\begin{aligned} Y_A^{\pi^+}(x,z)/A \propto\ & e_u^2 \cdot u_A(x) \cdot D_A^{fav}(z) + e_u^2 \cdot \bar{u}_A(x) \cdot D_A^{unfav}(z) \\ & + e_d^2 \cdot d_A(x) \cdot D_A^{unfav}(z) + e_d^2 \cdot \bar{d}_A(x) \cdot D_A^{fav}(z) \\ & + e_s^2 \cdot s_A(x) \cdot D_A^{s}(z) + e_s^2 \cdot \bar{s}_A(x) \cdot D_A^{s}(z), \\ Y_A^{\pi^-}(x,z)/A \propto\ & e_u^2 \cdot u_A(x) \cdot D_A^{unfav}(z) + e_u^2 \cdot \bar{u}_A(x) \cdot D_A^{fav}(z) \\ & + e_d^2 \cdot d_A(x) \cdot D_A^{fav}(z) + e_d^2 \cdot \bar{d}_A(x) \cdot D_A^{unfav}(z) \\ & + e_s^2 \cdot s_A(x) \cdot D_A^{s}(z) + e_s^2 \cdot \bar{s}_A(x) \cdot D_A^{s}(z), \end{aligned} \tag{6}$$

where $D_A^{fav,unfav,s}$ are the nuclear-FFs (nFFs) in the nucleus-A. One can then construct the charge-sum and charge-difference of the SIDIS data:

$$(Y_A^{\pi^+} \pm Y_A^{\pi^-})/A \propto [4(u_A \pm \bar{u}_A) \pm (d_A \pm \bar{d}_A)] \cdot [D_A^{fav} \pm D_A^{unf}], \tag{7}$$

where the strangeness part completely cancels in the charge-difference and is neglected in the charge-sum since we focus on $x > 0.1$. This will be more complicated in NLO.

2.1 Flavor-Dependent Medium Modification Effect in A=3 Nuclei

The EMC effect of ^{3}He has been well measured [9] [39]. However, such inclusive ratio measurements provide no insight into how individual quarks contribute to the EMC effect. In SIDIS with an additional flavor-tagging feature by detecting different hadrons produced by the knock-out quark, we can take the ratios of Eq. 7 among ^{3}He (labeled as "H"), ^{3}H (labeled as "T") and ^{2}D (labeled as "D"), and study the EMC effect of u- and $d-$quark individually:

$$R_{A_1/A_2}^{\pi,\pm}(x,z) = \frac{4(u_{A_1} \pm \bar{u}_{A_1}) \pm (d_{A_1} \pm \bar{d}_{A_1})}{4(u_{A_2} \pm \bar{u}_{A_2}) \pm (d_{A_2} \pm \bar{d}_{A_2})} \cdot \frac{D_{A_1}^{fav} \pm D_{A_1}^{unfav}}{D_{A_2}^{fav} \pm D_{A_2}^{unfav}} = A_{A_1/A_2}^{\pi,\pm}(x) \cdot B_{A_1/A_2}^{\pi,\pm}(z), . \tag{8}$$

More explicitly:

$$A_{H/D}^{\pi,+}(x) = \frac{4(u_H + \bar{u}_H) + (d_H + \bar{d}_H)}{5(u + \bar{u}) + 5(d + \bar{d})} = \frac{9(u_{p,H} + \bar{u}_{p,H}) + 6(d_{p,H} + \bar{d}_{p,H})}{5(u + \bar{u}) + 5(d + \bar{d})}, \tag{9}$$

$$A_{H/D}^{\pi,-}(x) = \frac{4(u_H - \bar{u}_H) - (d_H - \bar{d}_H)}{3(u - \bar{u}) + 3(d - \bar{d})} = \frac{7(u_{p,H} - \bar{u}_{p,H}) + 2(d_{p,H} - \bar{d}_{p,H})}{3(u - \bar{u}) + 3(d - \bar{d})}, \tag{10}$$

$$A_{T/D}^{\pi,+}(x) = \frac{4(u_T + \bar{u}_T) + (d_T + \bar{d}_T)}{5(u + \bar{u}) + 5(d + \bar{d})} = \frac{6(u_{p,T} + \bar{u}_{p,T}) + 9(d_{p,T} + \bar{d}_{p,T})}{5(u + \bar{u}) + 5(d + \bar{d})}, \tag{11}$$

$$A_{T/D}^{\pi,-}(x) = \frac{4(u_T - \bar{u}_T) - (d_T - \bar{d}_T)}{3(u - \bar{u}) + 3(d - \bar{d})} = \frac{2(u_{p,T} - \bar{u}_{p,T}) + 7(d_{p,T} - \bar{d}_{p,T})}{3(u - \bar{u}) + 3(d - \bar{d})}, \tag{12}$$

where u and d are free quark-PDFs, $u_{p,H}$ and $d_{p,H}$ is the u- and d-quark nPDFs in the proton of ^{3}He (analogous to other quarks' nPDFs). (This will be more complicated in NLO.)

As we can see, in the nuclear SIDIS data the nuclear modification effect not only exists in the PDFs (as measured by DIS data) but also can exist in the FFs. Shown in Fig. 4, the global analysis

of the nuclear-SIDIS data and pA collision-data given in Ref. [40] reveals significant medium effects of FFs in heavy nuclei which vary in z. In ^{4}He which is the lightest nucleus in this analysis, the nuclear effect, however, is not significant. For example, while the fit shows $\sim 1\%$ (5%) reduction at $z = 0.3$ ($z = 0.8$) with big error-bands, the data show no obvious z- and ν-dependence and the super-ratios are consistent with unity. Going from tightly bound ^{4}He toward A=3 nuclei of which the nuclear effects are significantly reduced based the inclusive DIS measurements [39], any nuclear effects in their FFs are very likely to be even smaller and will also be largely canceled in their ratios among ^{2}D, ^{3}H and ^{3}He.

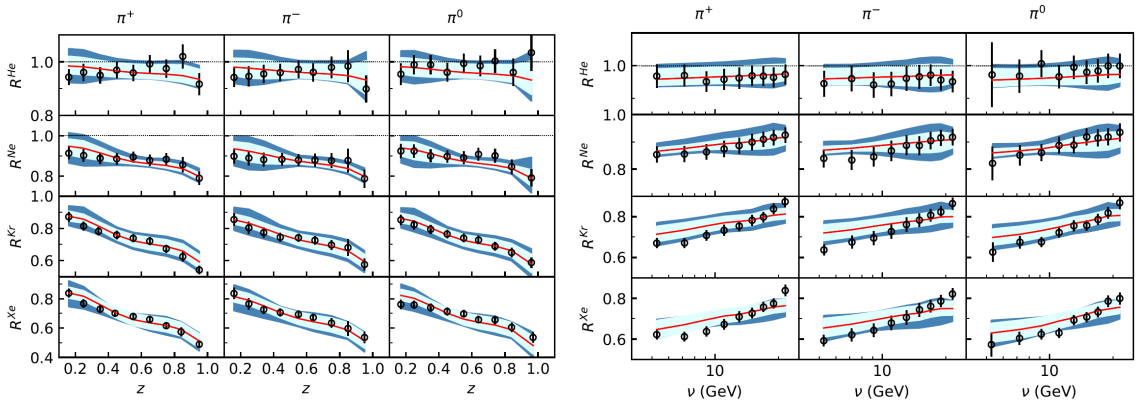

Figure 4: Global analysis of the super-ratios of multiplicity ratios ($R^h_A = M^h_A/M^h_D$, M^h_A is defined in Eq.13) from the HERMES SIDIS data [40]. The left (right) plot shows the z-(ν-)dependence. Red-lines are the fit and the light- (dark-) band is the errors at 68% (90%) confidence-levels.

Hence, even though the whole exercise in Eq. 8 is over-simplified based on the leading-order approximation, both the data and the global analysis suggest that such a simple approach,e.g. decoupling nPDFs and nFFs by varying x or z while fixing the other, should provide meaningful information of their flavor-dependent medium effect in the A=3 isotope and explore any unseen isovector effects. Our measurement can isolate the nuclear effect of PDFs in $A^{\pi,-}_{A/D}(x)$ by varying x while fixing the z-bin. $B^{\pi,-}_{A/D}(z)$ remains a constant when z is fixed and also can be independently measured as to be discussed below. If the EMC effect is only A-dependent (e.g. $u_{p,H} = u_{p,T}$), we can isolate the contributions from u- and d-quark nPDFs in the A=3 system using their different combination in Eq. 9 to Eq. 12. We also can study the possible isovector dependence of the EMC effect (e.g, $u_{p,H} \neq u_{p,T}$) by carefully measuring $R^{\pi,\pm}_{H/T}$ between ^{3}He and ^{3}H.

Similarly, we can measure the distribution of $B^{\pi,-}_{A_1/A_2}(z)$ by varying z while fixing the x-bin which allows us to study the medium modification effect in the FFs. When measuring the DIS cross-section simultaneously, we can construct the multiplicity ratio as:

$$M^h(z) = \frac{\sigma_{SIDIS}}{\sigma_{DIS}} \propto \frac{\sum_q e_q^2 f_1^q(x) \cdot D_q^h(z)}{\sum_q e_q^2 f_1^q(x)}. \tag{13}$$

So $B^{\pi,+}_{A/D}(z)$ can also be independently measured by taking the super-ratio of the sum of $\pi^\pm$ multiplicity-ratios:

$$B^{\pi,+}_{A/D}(z) = \frac{M^{\pi+}_A + M^{\pi-}_A}{M^{\pi+}_D + M^{\pi-}_D} = \frac{D^{fav}_A + D^{unfav}_A}{D^{fav}_D + D^{unfav}_D}, \tag{14}$$

which provides an independent way to decouple the FF contribution in Eq. 9 and Eq. 11.

We ultimately aim to provide high-precision cross-section data that can be included in the more sophisticated global analysis to extract the nPDFs and nFFs where high-order effects, nuclear effects, and other effects will be treated carefully.

2.2 Direct measurement of d/u ratios at high-x

As demonstrated in the MARATHON experiment [31, 36], the A=3 mirror nuclei can be used to study the F_2^p/F_2^n ratio using the super-ratio technique. The nuclear effects, which are both small and very similar in both nuclei, can be largely canceled in the ratio. The residuals, if any, can be carefully studied with advanced theoretical calculations. Such a technique can also be applied in the SIDIS data, such as in the PDF-only terms ($A_{H/T}^{\pi,\pm}$) in Eq. 8. In addition, as discussed in the previous sub-section, the FFs in A=3 isotopes, which could be different from their free counterparts, are also expected to be small and likely to be canceled in the ratios [40]. Therefore, we can treat: $u_{p,H} = u_{p,T} = u$ (and similarly for other light quarks), and also $D_H^{fav,unf} = D_T^{fav,unf}$, so Eq. 8 becomes:

$$R_{H/T}^{\pi,+} = \frac{9(u+\bar{u}) + 6(d+\bar{d})}{6(u+\bar{u}) + 9(d+\bar{d})}, \tag{15}$$

$$R_{H/T}^{\pi,-} = \frac{7(u-\bar{u}) + 2(d-\bar{d})}{2(u-\bar{u}) + 7(d-\bar{d})}, \tag{16}$$

which leads to:

$$\frac{d+\bar{d}}{u+\bar{u}} = \frac{9 - 6R_{H/T}^{\pi,+}}{9R_{H/T}^{\pi,+} - 6} \tag{17}$$

$$\frac{d-\bar{d}}{u-\bar{u}} = \frac{7 - 2R_{H/T}^{\pi,-}}{7R_{H/T}^{\pi,-} - 2}. \tag{18}$$

Eq. 18 provide the most direct way to measure the d/u ratio which traditionally relies on the measurement of the DIS cross-sections (σ_p/σ_n) which contain contributions from all quark-flavors and also suffer from large uncertainty due to the treatment of the "effectively-free" neutrons in light nuclei. When x is close to 1, the contributions of $\bar{u}$ and $\bar{d}$ can be ignored, then we have an interesting equality that can be used experimentally:

$$\frac{d}{u} \simeq \frac{9 - 6R_{H/T}^{\pi,+}}{9R_{H/T}^{\pi,+} - 6} = \frac{7 - 2R_{H/T}^{\pi,-}}{7R_{H/T}^{\pi,-} - 2}, \text{ when } x \to 1 \tag{19}$$

At leading-order approximation, the z-dependence in $R_\pi^\pm$ is omitted in the ratios where the FFs are completely canceled. However, such z-dependence could only be partially canceled at higher-order. By binning the data in multiple z-bins, we can examine the variation among different z-bins by independently measuring $B_{H/T}^{\pi,\pm}(z)$ (similar to Eq. 14) and extract the d/u ratio in the advanced global analysis. With the high-luminosity and large acceptance experimental setup, such a novel technique using SIDIS is likely to produce the cleanest results of the d/u ratio that alternatively can only be obtained from the parity-violation DIS measurement [41] which has greater experimental challenges.

2.3 Three-Dimensional Structures of A=3 Nuclei

Understanding the three-dimensional structure of the nucleon is one of the key physics programs in the JLab 12GeV era as well as for the future Electron-Ion Collider (EIC). Measurements of the

SIDIS asymmetries with polarized protons and ^{3}He (as effective neutron targets) have been proposed for CLAS12 [42], SoLID [43], and the future EIC [44] to study Transverse Momentum Distributions (TMDs) that allow access to the spin and orbital angular momentum of individual quarks in nucleons. The SIDIS asymmetries can only link to TMDs when combined with the unpolarized SIDIS cross-sections, e.g., the transversely polarized single-target asymmetry, $\delta\sigma_{UT}^{SIDIS} = \sigma_{UU}^{SIDIS} \cdot A_{UT}$. However, many experiments mainly focus on precision measurement of SIDIS asymmetries with different beam and target polarization, while the unpolarized cross-sections σ_{UU}^{SIDIS} presumably rely on other independent measurements with more precise data.

The unpolarized SIDIS structure function with additional p_T-dependence becomes:

$$F_{UU}(x, z, P_T) = \sum_q e_q^2 [f_1^q(x, k_\perp) \otimes D_q^h(z, q_T)], \tag{20}$$

where P_T is the transverse momentum of the detected hadron, $k_\perp$ is the initial transverse momentum of the quark before being knocked out, and q_T is the final transverse momentum of the struck quark before hadronization happens[1]. The symbol $\otimes$ reveals that $k_\perp$ and q_T, which can not be experimentally accessed, are highly correlated. P_T is the only experimental observable can link to the other two quantities at a leading-order approximation:

$$\vec{P}_T = z\vec{k}_\perp + \vec{q}_T + O(k_\perp^2/Q^2). \tag{21}$$

Up until now, the exact forms of the $k_\perp$ distributions in TMDs and the q_T distributions in FFs are largely unknown. The most common approach in the global analysis of the SIDIS data is to assume a Gaussian-like distribution for the transverse component of both the TMDs and FFs [45,46], e.g.:

$$f_1^q(x, k_T) = f_1^q(x) \frac{1}{\pi < k_T^2 >} exp(-\frac{k_T^2}{< k_T^2 >}), \tag{22}$$

$$D_1^q(z, q_T) = D_1^q(z) \frac{1}{\pi < q_T^2 >} exp(-\frac{q_T^2}{< q_T^2 >}), \tag{23}$$

With this Gaussian ansatz, we can decouple the convolution into the product of

$$F_{UU}(x, z, P_T) = \sum_q e_q^2 f_1^q(x) \cdot D_q^h(z) \cdot exp(-\frac{P_T}{< P_T^2 >}), \tag{24}$$

where $< P_T^2 >= z^2 < q_T^2 > + < k_T^2 >$. Such an approximation has been widely used in the SIDIS community and is applied in the simulation of this proposal. However, this approximation could be an oversimplification. For example, the same Gaussian width is usually applied to all quark-flavors, while some studies show that the distribution-widths can be different among quark-flavors [45, 47]. Another study suggests that the $< P_T^2 >$ also has sizable x-dependence [48]. Some analyses even observe the non-Gaussian behavior of the P_T-distributions [49].

With highly precise 4D SIDIS data we are able to perform a global analysis, with the help from theoretical models, to systematically decouple $f_1^q(Q^2, x, k_\perp)$ from $D_1^q(Q^2, x, q_T)$ in the SIDIS structure functions. One also can further study the azimuthal distribution of the unpolarized SIDIS events (ϕ) which provides precious information on the Boer-Mulder TMD as well as the high-order and high-twist QCD effects [50].

The FF distributions are usually measured via (e^+, e^-) reactions such as BELLE [51]. However, neither the precision nor the timeline of the future (e^+, e^-) measurements fits the need for a multiple-dimensional TMD study in the upcoming SIDIS experiments. It is crucial to carry out a dedicated

[1] In this proposal, $k_\perp$ represents the initial quark transverse momentum, p_T and q_T are defined as the transverse momentum of the detected hadron and the knocked-out quark. In some literature, people use $P_{h\perp}$ as the transverse momentum of the detected hadron and P_T as the final transverse momentum of the knocked-out quark.

high-precision measurement of FFs using SIDIS and perform a global analysis to extract FFs in collaboration with the theoretical community. The study of the SIDIS pion- and kaon-production with unpolarized ^{3}He and ^{3}H provides a great opportunity to measure unpolarized TMDs and unpolarized FFs in support of other SIDIS measurements that will extract all other TMDs using polarized targets.

Under isospin symmetry, we can separate the TMD and FFs for individual light quarks from the SIDIS data. We can carefully examine the P_T distributions of different quark flavors. The precise determination of their TMDs and FFs, combined with good theoretical control to minimize the nuclear effect in the A=3 mirror nuclei, can be directly applied to the studies of other TMDs measured by polarized proton and neutron targets. When comparing the TMDs and FFs in the A=3 system with ones in the deuterium nucleus, we can further study the medium effect on the transverse direction which opens up a completely new angle to understand the EMC effect.

2.4 Factorization

A key assumption in the measurement of the quantities described in Sections 2.1-2.3 is that the semi-inclusive meson production process factorizes, i.e., the interaction of the virtual photon with the struck quark proceeds independent of the hadronization process. There is some evidence from the 6 GeV Jefferson Lab program that this is approximately true for certain kinematics. Experiment 00-108 in Hall C found that SIDIS cross-sections for π^+ and π^- production from hydrogen and deuterium were consistent with a simple parametrization of the SIDIS cross-sections that made use of PDFs and a parametrization of fragmentation functions from high energy data (see Fig. 5, left). The same experiment also examined combinations of π^+ and π^- cross-sections from hydrogen and deuterium (Fig. 5, right);

$$\frac{\sigma_p(\pi^+) + \sigma_p(\pi^-)}{\sigma_d(\pi^+) + \sigma_d(\pi^-)} = \frac{4u(x) + 4\overline{u}(x) + d(x) + \overline{d}(x)}{5[u(x) + d(x) + \overline{u}(x) + \overline{d}(x)]} \tag{25}$$

and

$$\frac{\sigma_p(\pi^+) - \sigma_p(\pi^-)}{\sigma_d(\pi^+) - \sigma_d(\pi^-)} = \frac{4u_v(x) - d_v(x)}{3[u_v(x) + d_v(x)]}. \tag{26}$$

Assuming independent factorization, these ratios should depend only on the quark PDFs and be independent of z. This was found to be true at $x = 0.3$, up to $z = 0.7$ for E10-108.

Experiments 12-09-017 and 12-09-002 will provide similar cross-section and ratio information over a larger range in x and Q^2 with high precision. This information will provide information about the extent to which factorization holds and provide information regarding our understanding of the SIDIS reaction mechanism, both at the cross-section level and in observables involving the ratios of targets. In addition, the large acceptance of the CLAS spectrometer will allow simultaneous examination of the Q^2 and z dependencies at fixed x to directly test assumptions about factorization.

2.5 Hadron attenuation

Similar to the modification of quark distributions in nuclei, the probability for a quark to hadronize into a particular meson or nucleon will also undergo modification in the nucleus. This is particularly true for an underlying diquark description of the EMC-SRC effect [53]. If these nuclear effects on the fragmentation process are large enough, they could potentially complicate measurements of initial state nuclear modifications via the SIDIS reaction.

Final-state nuclear effects in fragmentation are generally measured via the hadron attenuation ratio, in which the nuclear SIDIS cross-section (normalized to the inclusive electron cross-section) is compared to that from the deuteron;

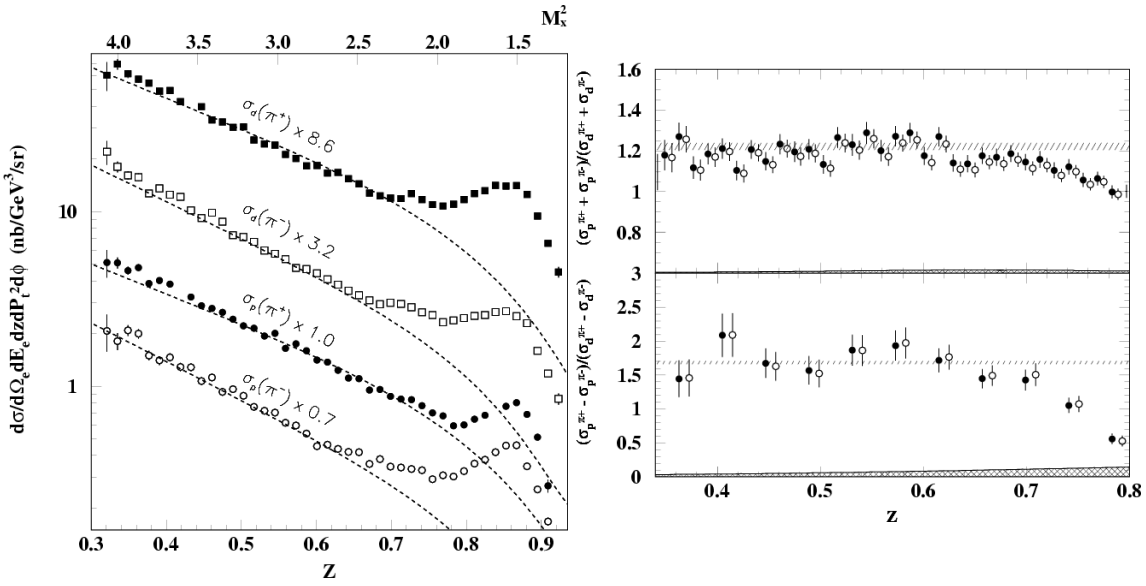

Figure 5: SIDIS cross sections (left) and charge sum/difference ratios (right) for π^+ and π^- production from H and D from Hall C experiment E10-108 [52]

$$R_h(z,\nu) = \frac{\left(\frac{1}{\sigma}\frac{d\sigma}{dzd\nu}\right)_A}{\left(\frac{1}{\sigma}\frac{d\sigma}{dzd\nu}\right)_D} = \frac{\left(\frac{1}{N_e}\frac{dN_h}{dzd\nu}\right)_A}{\left(\frac{1}{N_e}\frac{dN_h}{dzd\nu}\right)_D} \,. \tag{27}$$

Hadron attenuation effects have been measured both at HERMES [54] and Jefferson Lab [55]. In particular, such effects display a dependence on z and ν, with measurable differences in the distribution in p_T.

Hadron attenuation effects in $A = 3$ nuclei are expected to be small (see the ^{4}He results in Fig. 6) and similar for ^{3}He and ^{3}H. Measurements at $x = 0.3$, where initial state nuclear effects (i.e. the EMC effect) are expected to be small, will allow the experiment to map out the ν, z and p_T dependence of nuclear effects in fragmentation and apply that information at larger x, where the EMC effect is larger.

3 Experimental Setup

We will use the standard configuration CLAS12 detector and a 10.6 GeV beam incident on identical ^{2}D, ^{3}He, and ^{3}H target cells to measure $(e, e'\pi^+)$ and $(e, e'\pi^-)$. It is very important to use identical cell for all three targets in this proposal to minimize the systematic uncertainties. The scattered electron and the ejected pions will be detected in the forward detector. If the RICH upgrade is complete, then we will also measure $(e, e'K^\pm)$, but that is not the major goal of this proposal. To minimize the systematic uncertainty due to the different acceptance of positive and negative charged particles, we will regularly flip the polarity of the CLAS12 torus.

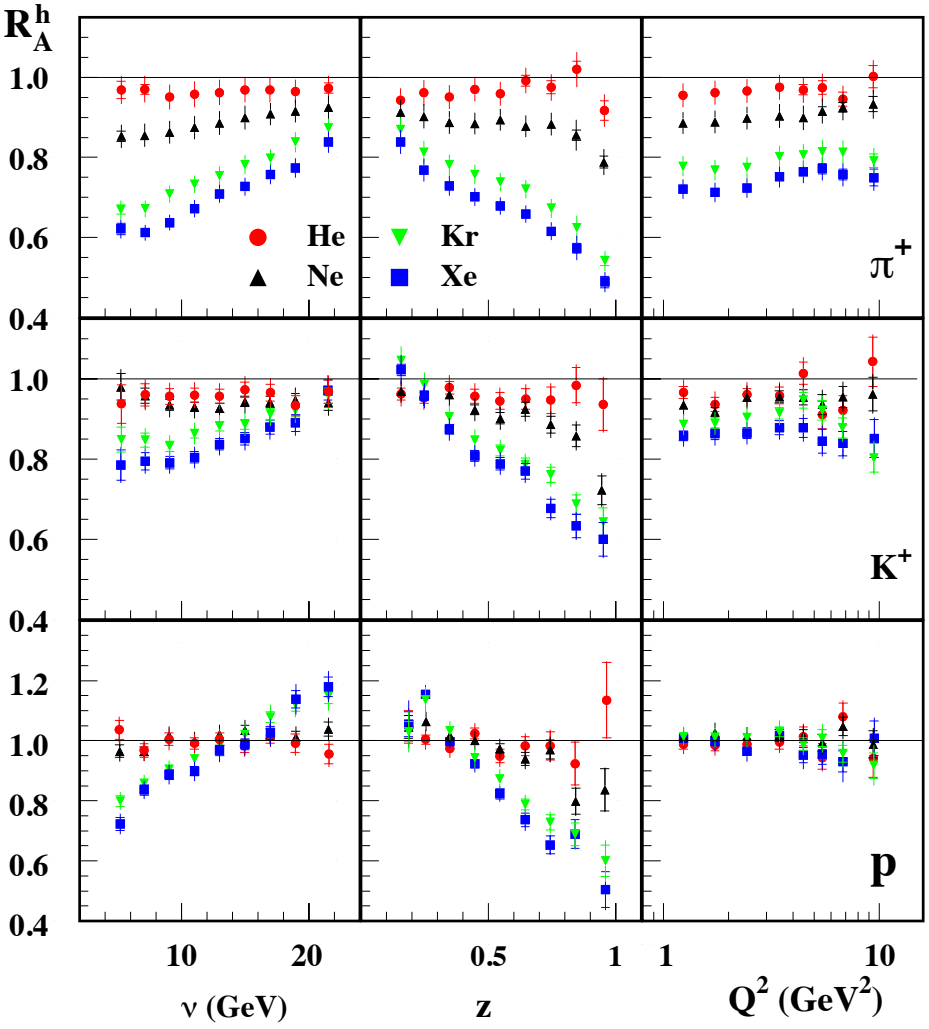

Figure 6: Hadron attenuation ratios from HERMES [54] for π^+ production. Note the modest effects for ^{4}He.

3.1 Target System

We propose the same target system planned for the approved new Tritium-SRC experiment (E12-12-005 [1]). With the limitation of the maximum luminosity of CLAS12 (1.35×10^{35} $nucleons{\cdot}cm^{-2}{\cdot}s^{-1}$) and the relatively thick aluminum cell and chamber, the effective luminosity of the Tritium target is 3.45×10^{34} $nucleons \cdot cm^{-2} \cdot s^{-1}$. In order to minimize the systematical uncertainties we will use identical cells for all three targets. The same effective luminosity is used for ^{2}D and ^{3}He in the rate estimation for this proposal. Some details of the proposed target system design are given in Appendix A.

3.2 Kinematics Coverage

The large acceptance of CLAS12 allow us to have a wide coverage of important physics variables $0.05 < x < 0.7$, $1 < Q^2 < 9$ $(\mathrm{GeV}/c)^2$, $0.3 < z < 0.8$ and $0 < P_T < 1.3$ GeV/c. The kinematic coverage for π^- and π^+ can be seen in Figs. 7–9. We will use the CLAS12 vertex resolution to eliminate events originating from the target walls.

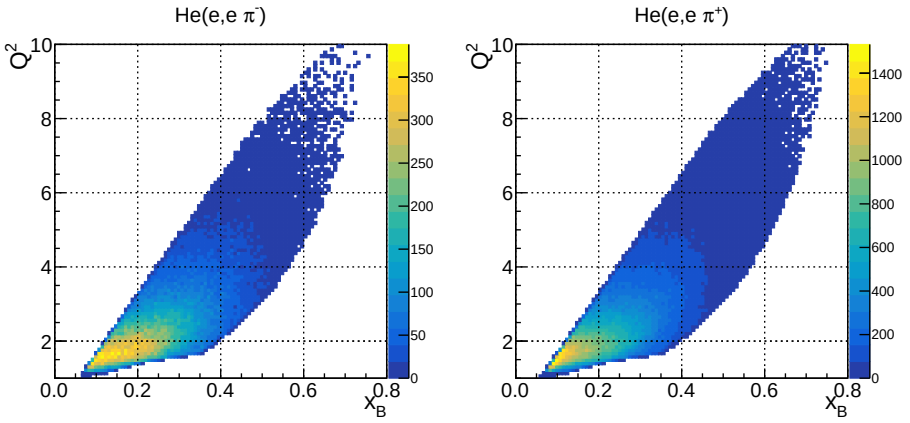

Figure 7: x and Q^2 coverage of π^+ and π^- from ^{3}He

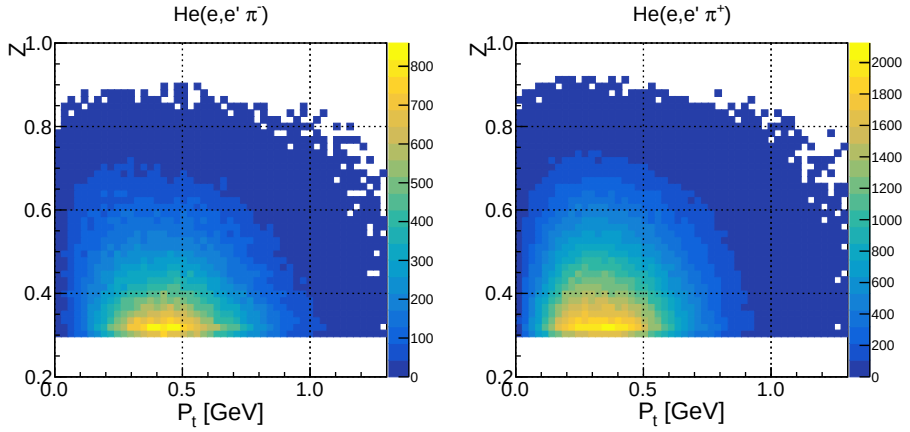

Figure 8: z and P_t coverage of π^+ and π^- from ^{3}He, $z \geq 0.3$.

4 Experimental Projection

4.1 Monte-Carlo Simulation and rate estimation

Detailed Monte-Carlo Simulations for SIDIS processes were performed using the full CLAS12 simulation and reconstruction chain. Unpolarized SIDIS events were generated with the CLASDIS generator, digitized using GEMC, and reconstructed with the latest available (v.6.5.3) clara/coatjava reconstruction framework. The reconstructed events from the CLAS12 simulation for the in-bending setting were used as pseudo-data to estimate the rates and the projected statistical uncertainty in the

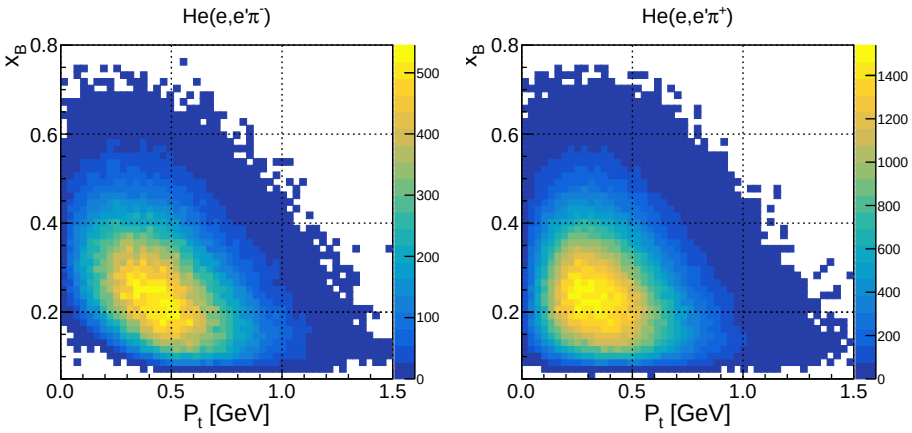

Figure 9: x vs P_t coverage of π^+ and π^- from ^{3}He

proposed observable. The SIDIS rates for ^{2}D, ^{3}H, and ^{3}He were obtained by combining simulations for the proton and neutron separately, thus neglecting any nuclear effects.

SIDIS events were selected by applying the standard cuts: $Q^2 > 1$ (GeV/c)^2, $W^2 > 4$ (GeV/c)^2, $0.1 < y < 0.85$, and $0.3 < z < 0.8$. These cuts are commonly used in the SIDIS global analysis as well as in the proposed JLab 12GeV experiments. In addition we required $\theta_e > 8^\circ$ and $P_e > 2$ to make sure electrons are in the good acceptance region in forward detector. An overall 80% detector efficiency is applied to the simulated events. The pseudo-data events that pass the selection cuts were binned in physics variables such as x. The number of events in each bin were determined and scaled to the total integrated luminosity for each target. The statistical relative uncertainty for each bin was calculated as $1/\sqrt{N}$.

4.2 Flavor-Dependence Nuclear Effect in A=3

As discussed in Sec. 2.1, the flavor-dependent EMC effect in light-quarks can be directly studied in SIDIS by measuring the observables shown in Eq. 8. In the generator, the same sets of FFs are used in calculating SIDIS cross-sections of ^{2}D, ^{3}H and ^{3}He, so the FF-only terms ($B^{\pi,\pm}_{A_1/A_2(z)}$) are basically unity. While the FFs of these nuclei are expected to be similar and will also be studied exclusively in this proposal, we can assume the ratios are directly related to the PDF-only term by fixing the z-bin, i.e. $R^{\pi,\pm}_{A_1/A_2} = A^{\pi,\pm}_{A_1/A_2}$.

In this proposal, we adopt the EMC slope of $\sigma^{^3He}_{DIS}/\sigma^{^2D}_{DIS}$ measured by SLAC [9] with additional 5% correction to the slope to match the Hall-C result [39]. We apply the corrected EMC slope (SLAC Fit) to the free-PDF of each quark with the assumption of no flavor-dependent of the EMC effect (e.g,$u_A/u = d_A/d$), and also assume the same nuclear effect in ^{3}H and ^{3}He (e.g. $F_2^H = F_2^T$) which has been suggested by the preliminary MARATHON results [56]. As a comparison, we also include the KP model [57] used in the recent MARATHON analysis [31] to describe the different medium effects in both ^{3}H and ^{3}He, and we still assume the medium effect is identical for all quark-flavors in each nucleus. We can construct the SIDIS structure functions (shown in Eq. 2) using these flavor-independent nuclear-PDFs. No existing theoretical calculations are available to describe how individual quarks are modified in various nuclei; we are actively discussing with several theory groups for theoretical calculations on the flavor-dependent EMC effect in the A=3 system [58]. Considering the dearth of theoretical models we adopt a simplified approach: the EMC effect observed in the

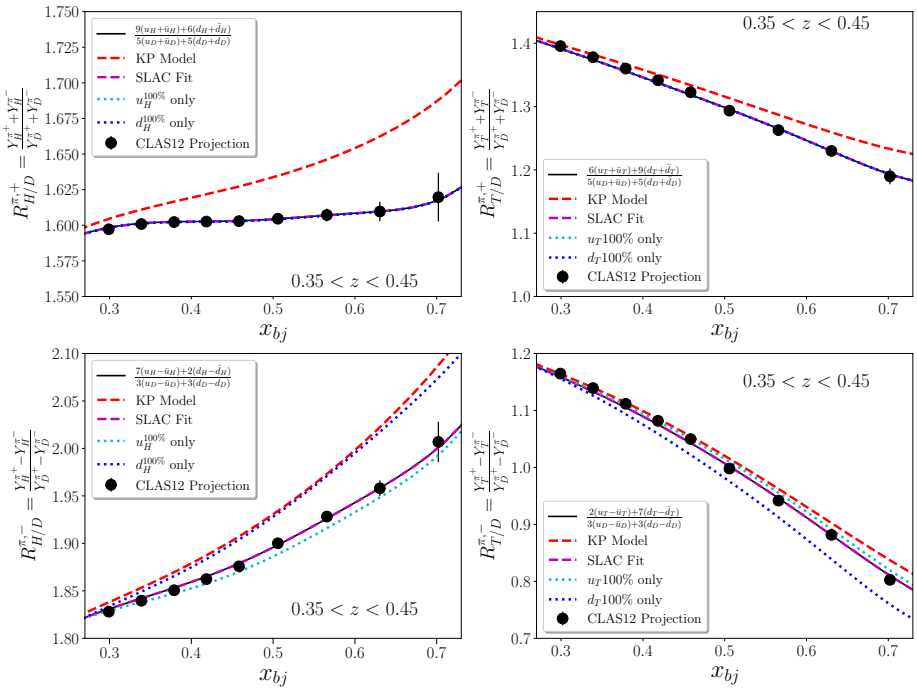

Figure 10: Projected ratios of $\pi^{\pm}$ yield-sum and yield difference between ^{3}H (^{3}He) and ^{2}D. Dashed line $R^{\pi,\pm}_{A/D}$ are calculated with the SIDIS structure functions constructed based on Eq. 9-11-10-12 with various nuclear-PDF models discussed in the text. The data points are based on the SIDIS MC events with standard SIDIS cuts and one fixed z-bin ($0.35 < z < 0.45$) and only contain the statistical errors.

DIS reaction is solely due to the medium modification only to u- or d-quark, for example:

$$F_2^{A,SLAC} = (Ze_u^2 + Ne_d^2)(u_{p,A}^{100\%} + \bar{u}) + (Ze_d^2 + Ne_u^2)(d + \bar{d}) + (Z+N)e_s^2(s+\bar{s}), \quad (28)$$

$$= (Ze_d^2 + Ne_u^2)(d_{p,A}^{100\%} + \bar{d}) + (Ze_u^2 + Ne_d^2)(u + \bar{u}) + (Z+N)e_s^2(s+\bar{s}), \quad (29)$$

where $F_2^{A,SLAC}$ are calculated with free-PDFs (u,d,s,...) corrected by the ^{3}He EMC slope. Hence we construct a "pseudo-model" where $u_{p,A}^{100\%}$ ($d_{p,A}^{100\%}$) serves as the extreme case where the medium effect in A is 100% on u (d) only (other quark-PDFs remain free). Two assumptions are made in this "pseudo-model": one is the same quark-flavor is modified similarly in protons and neutron, and the other is that the EMC effect in all quarks always causes the reduction of the structure function which may not be necessary true for all quarks (e.g., there could be a cancellation effect among different quarks). We then applied these nuclear-PDFs (KP-model, SLAC-Fit, and the "pseudo-model") to calculate the proposed SIDIS observable. The projected results are shown in Fig. 10 where the data were binned in x after the standard SIDIS cuts, fixing $0.35 < z < 0.45$ and not cutting on P_T. The statistical uncertainty in each data point is calculated based on the number of MC events in each x-bin for each measurement.

$R^{\pi,+}_{H/D}$ and $R^{\pi,+}_{T/D}$ are not sensitive to the nuclear effects modeled by the flavor-independent SLAC Fit and the flavor-dependent "pseudo-model" ($u_{p,A}^{100\%}$, $d_{p,A}^{100\%}$). However, the curves calculated with KP-model stand out, suggesting that the observable may be sensitive to any iso-vector effect in the EMC. On the other hand, $R^{\pi,-}_{H/D}$ and $R^{\pi,-}_{T/D}$ are sensitive to the different models and should thus be sensitive to a flavor-dependent EMC effect. These four observables will be measured simultaneously and allow us to explore various scenarios of the flavor-dependent EMC effect in the $A = 3$ nuclei.

4.3 d/u Ratios

Fig. 11 shows the experimental projection of the $\frac{d+\bar{d}}{u+\bar{u}}$ (left) and $\frac{d-\bar{d}}{u-\bar{u}}$ (right) based on Eq. 18. Even though a majority of the events are rejected by the SIDIS cuts and the z cuts, the statistical uncertainties are still small enough even at very high x thanks to the wide acceptance of CLAS12. The curves are calculated from the PDF models discussed in the previous section. As expected, nuclear effects largely cancel in the sum ratio, $\frac{d+\bar{d}}{u+\bar{u}}$, even in the very extreme cases ($u_{p,A}^{100\%}$ and $d_{p,A}^{100\%}$); thus the ratios are almost identical to those calculated with free-PDFs. These effects do not cancel in the difference ratios, $\frac{d-\bar{d}}{u-\bar{u}}$, which could be sensitive to the the extreme cases. When $x > 0.5$, the contribution from sea-quarks are negligible and the values of these sets of ratios become identical.

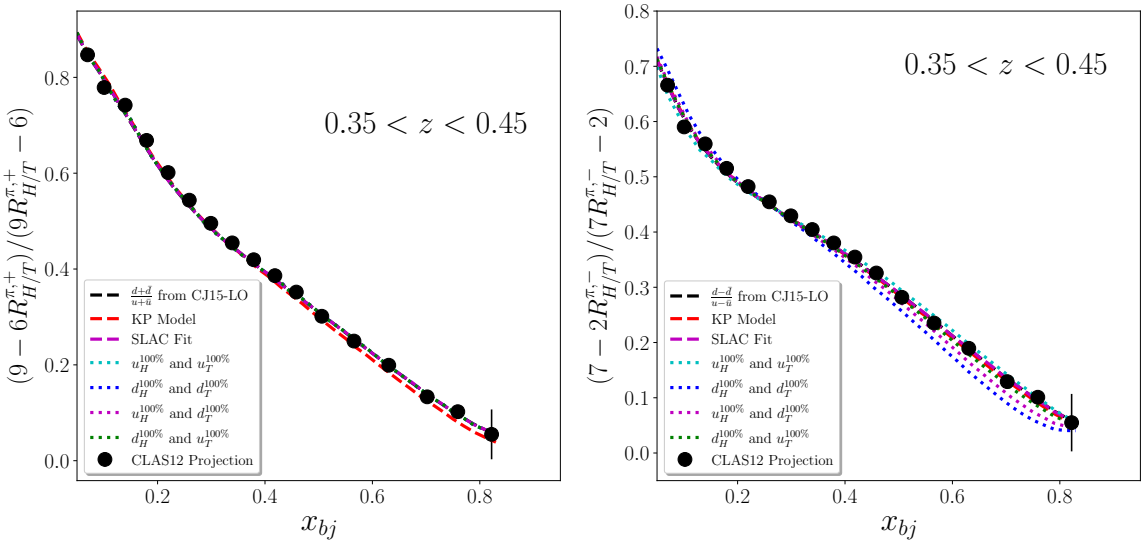

Figure 11: Projected d/u ratios. The mean x values (statistical errors) of the highest three data points in this projection are: 0.70 (1.1%), 0.76 (2.7%) and 0.82 (9.5%). Statistical errors only. Additional 2% systematic uncertainties are not included in the error-bars.

4.4 3D Measurement of A=3 Nuclei

As discussed in Sec. 2.3, SIDIS data in this proposed measurement will allow theorists and phenomenologists to extract the unpolarized TMDs and FFs in A=3 nuclei and perform the flavor separation, a set of extremely beneficial results for the TMD program at JLab and elsewhere. To illustrate the high quality of our future data, we bin the SIDIS data in (Q^2, x, z, P_T) defined by the bins below:

$$
\begin{aligned}
Q^2 \text{ bins}[4] &= [(1.0-2.0),\ (2.0-3.5),\ (3.5-5.5),\ (5.5-10)]\ \text{GeV}^2,\\
z \text{ bins}[6] &= [(0.3-0.35),\ (0.34-0.4),\ (0.4-0.45),\ (0.45-0.5),\ (0.5-0.6),\ (0.6-0.7)],\\
P_T \text{ bins}[6] &= [(0.0-0.2),\ (0.2-0.4),\ (0.4-0.6),\ (0.6-0.8),\ (0.8-1.1),\ (1.1-2.0)]\ \text{GeV/c},\\
x \text{ bins}[10] &= [(0.04-0.08),\ (0.08-0.12),\ (0.12-0.16),\ (0.16-0.2),\ (0.2-0.26),\\
&\qquad (0.26-0.32),\ (0.32-0.4),\ (0.4-0.5),\ (0.5-0.65),\ (0.65-0.95)].
\end{aligned}
$$

Fig. 12 shows the multiple dimensional binning of the ^{3}H pion-SIDIS data (^{2}D and ^{3}He have similar projection results). Data points with statistical uncertainties larger than 10% are removed from the plots. One can see the projected data cover a wide range of each kinematic quantity but

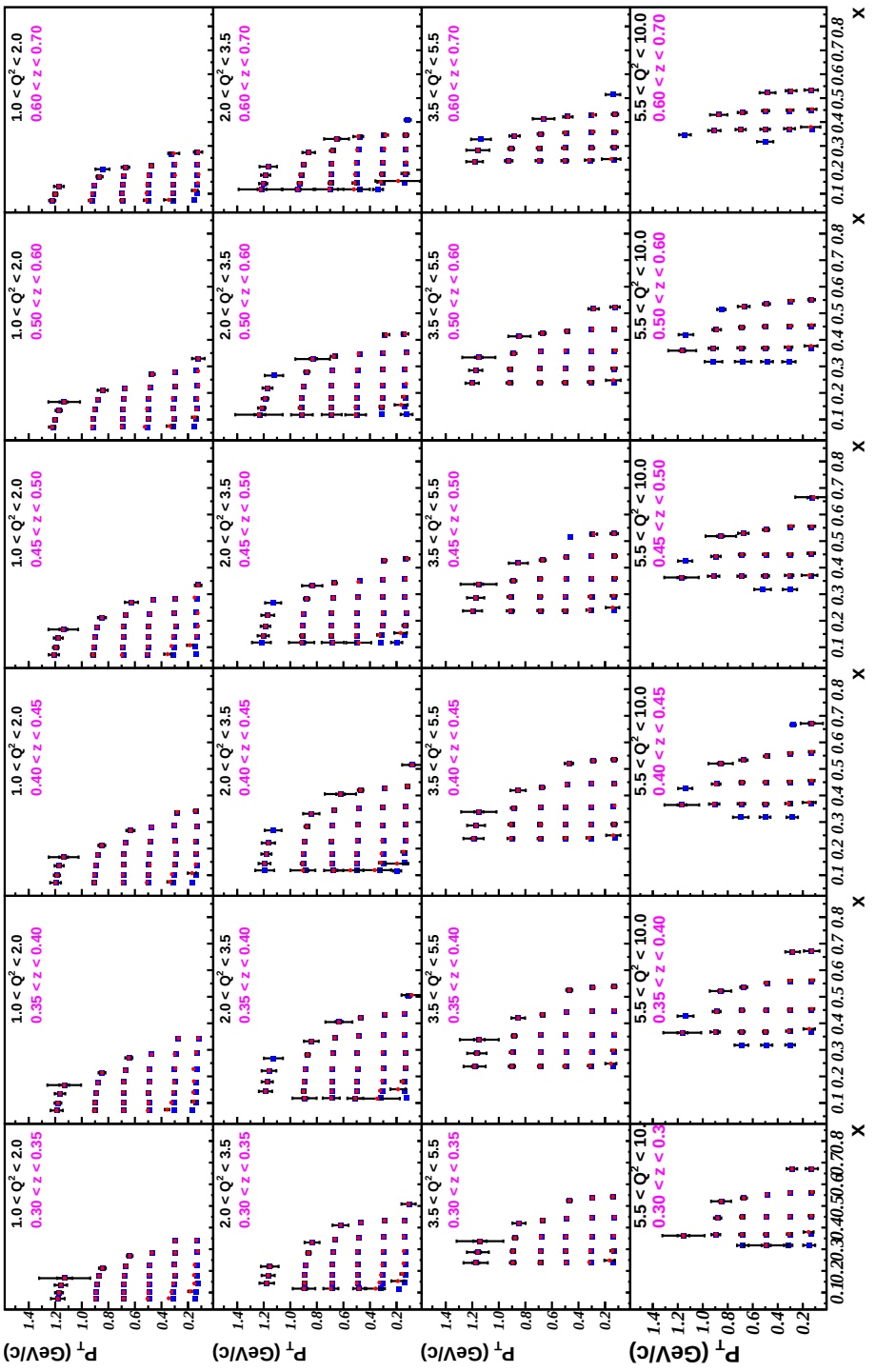

Figure 12: Projected H3 Pion-SIDIS data binned in 4D. Blue (red) dots are π^+ (π^-).

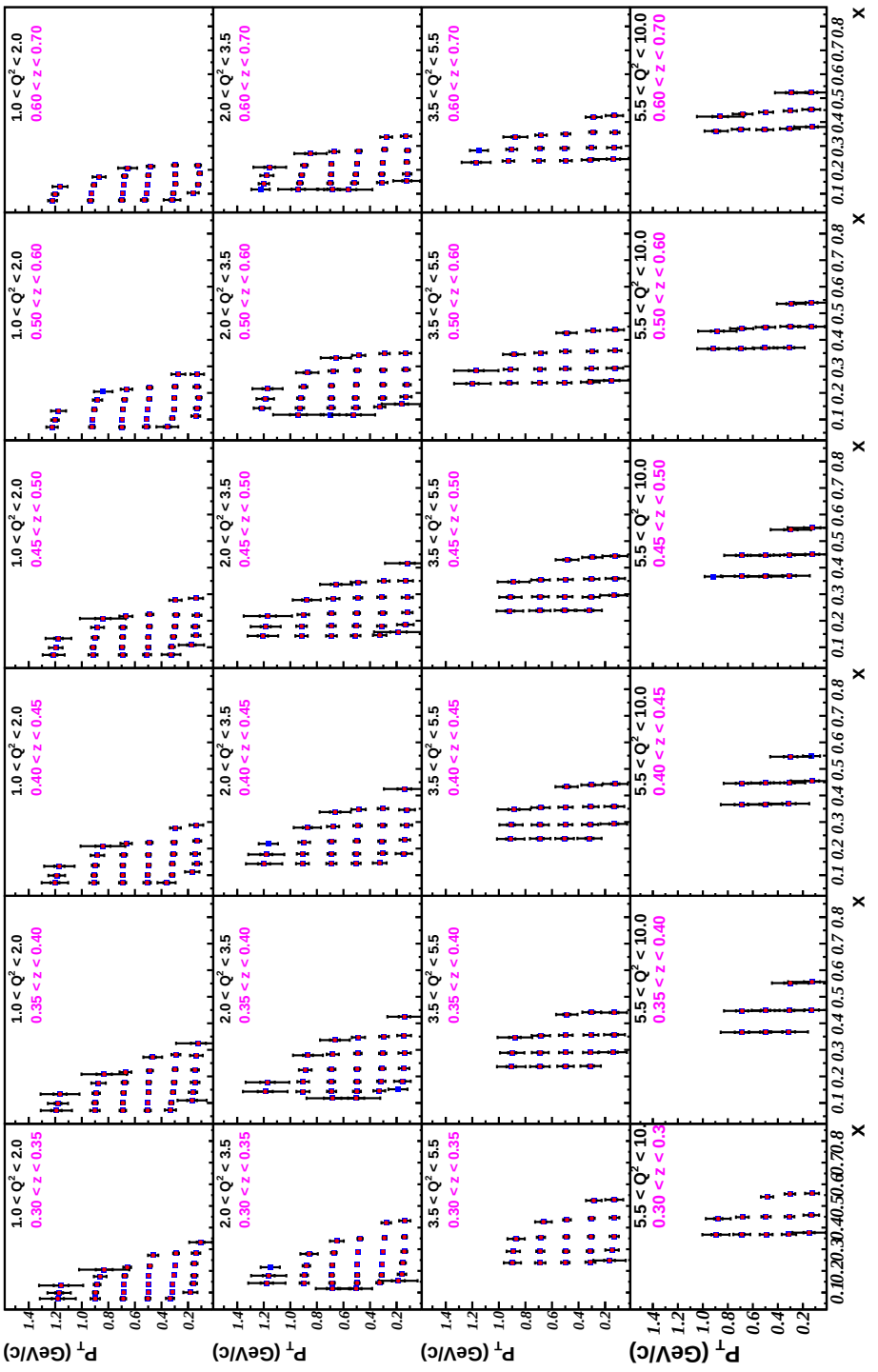

Figure 13: Projected H3 Kaon-SIDIS data binned in 4D. Blue (red) dots are K^+ (K^-).

remain high precision. These data will provide enormous value to the TMD community for the study of the factorization theorem, the hadronization process, and most importantly, the global analysis of exacting TMDs and FFs. The kaon-SIDIS projection plots are shown in Fig. 13 with the same binning. While the binning will be optimized during the real data analysis, the plots suggest that the kaon data will be highly valuable to study the kinematic region of the current fragmentation region and also provide information about the strangeness content in the 3D structure of A=3 nuclei.

4.5 Beam Time Request

The number of beam days (PAC) per target is listed in the Table. 1. We request 20 PAC days of beam time for each $A = 3$ target. This will ensure high statistical precision, below 1%, in the range of $0.3 < x < 0.7$ for both $(e, e'\pi^-)$ and $(e, e'\pi^+)$ for the EMC flavor dependence study (Fig. 10). This beam time will also allow us to have enough statistical precision for the d/u measurement up to $x > 0.75$ (Fig.11), and to allow multi-dimensional binning for the study of 3D nuclear structure (Fig. 12, 13). The deuterium data is crucial for this proposal to study nuclear effects with an identical target cell. Therefore, we request 10 PAC days of running on the deuterium target, (50% of the statistical precision compared to $A = 3$ targets). We will also use hydrogen to optimize our calibration which requires 1 PAC days.

The charge-dependent acceptance correction for pions, (π^+ vs. π^-), is expected to be one of the main sources of systematic uncertainty. In order to decrease this uncertainty, we will flip the torus polarity eight times each for $A = 3$ and four times for deuterium. At 2.5 hours per polarity reversal, this will take 50 hours, or two calendar days (1 PAC day).

In addition, we request 2 PAC days for target changing. It takes at least 3 shifts (0.5 PAC day) for Tritium target changing, and 1 to 2 shifts for ^{3}He and ^{2}D targets. We also include 5 PAC days for other calibrations such as the beam calibration (0.5 PAC day), empty target runs (2 PAC days, 5% of physics data) and luminosity scan, efficiency studies (1.5 PAC days), and H normalization.

Table 1: Requested beam time per target, including calibration time, changing magnetic polarity and target change overhead.

Target:	^{2}**D**	^{3}**He**	^{3}**H**	**Total**
Measurement Days (10.6 GeV)	10	20	20	**50**
Calibration: Luminosity, dummy, H				**5**
Target Changes				**2**
Torus polarity reversals				**1**
			Total at 10.6 GeV:	**58**

As detailed in Appendix A, the effective luminosity of all three targets are 3.45×10^{34} nucleon/cm$^2/s$ which corresponds to a beam current of 110 nA. This low beam current does not require the raster and is expected to have a negligible effect on the target density.

4.6 Systematic Uncertainties

The physics measurements of this proposal are based on the ratios of pion yields ($\pi^+ \pm \pi^-$) from two different targets (see Fig. 10), in which many systematic uncertainties largely cancel. We will use some of the techniques pioneered by the CLAS Two-Photon Exchange (TPE) experiment [59]. We will use identical target cells for the different target gases. In order to make sure that the π^+ and π^- acceptances are the same we will flip the Torus polarity frequently. We will use fiducial cuts to determine the regions of common acceptance for in-bending and out-bending electrons and for in-bending and out-bending pions. We will monitor the detector imperfection uncertainty (including the effects of the fiducial cuts) by measuring the variance in the ratios from the six independent

CLAS12 sectors (specifically from detecting the electron in each of the six sectors). By flipping the torus polarity often, we will reduce the effects of any charge dependent track reconstruction. The random coincidence background will be suppressed to below 0.5% by the low luminosity and by demanding a common e^- and π vertex. Based on the TPE analysis [59], we expect to control the point-to-point systematic uncertainties in the ratios to better than 1% (see Table 2).

We anticipate normalization uncertainties in the ratio of about 2.5% due to target thickness uncertainties of 1.5% each, beam-charge measurement run-by-run stability (1%), and tritium decay correction (0.15%) [60].

	Sectors	Tracking	Vertex	Fiducial	Acceptance
Uncertainty (%)	0.34	0.13	0.16	0.41	0.1

Table 2: The systematic uncertainties of the $(e^+, e^{+'}p)/(e^-, e^{-'}p)$ ratio in the CLAS Two-Photon Exchange experiment [59]. "Sectors" refers to the 6-sector ratio variance, "tracking" refers to the CLAS charge-dependent tracking, "vertex" refers to the effect of different vertex cuts, "fiducial" refers to the effect of narrowing the fiducial cuts, and "acceptance" refers to the maximum variance in the acceptance correction factors determined from monte carlo simulation. Since the TPE systematic uncertainties were determined by statistical measurements, we used the data bins with the greatest statistical precision for this table.

5 Conclusion

We propose to measure the SIDIS reaction with ^{2}D, ^{3}H and ^{3}He using a 10.6 GeV unpolarized electron beam and the standard configuration CLAS12 detector. We will use the same Tritium target system to be used by the approved CLAS12 Tritium-SRC experiment (PR12-20-005). We request 50 PAC days of physics running plus an additional 8 PAC days for calibration, target changes, and magnet flipping. The high-precision SIDIS data on A=3 mirror nuclei will provide great insight into the flavor-dependence of the EMC effect in nuclei which will greatly improve upon purely inclusive measurements. Thanks to the usage of the mirror isotopes with well-controlled nuclear effects, we can perform a direct measurement of the d/u ratio at high-x. The wide kinematic coverage and high count-rates allow us to perform 4D binning of the SIDIS data in all three nuclei which allows theorists to use this data to test factorization in SIDIS, understand how the struck quark hadronizes, and to study the transverse components of different quark-flavors. Ultimately we hope to extract the TMDs and FFs in $A = 3$ nuclei and reveal, for the first time, their nuclear effects. Such a measurement is essential to the entire TMD program at JLab and for the future Electron-Ion Collider. If the RICH is available for this experiment, we can also measure kaon-SIDIS data which provides a unique data set to study the kinematic definition of the current fragmentation region as well as to probe strangeness in the $A = 3$ system. We anticipate that this rich data set will encourage theorists to provide detailed exact calculations of SIDIS in these light nuclei.

6 Other Physics Opportunities as Run-Group Measurements

The proposed experiment contains other important physics channels. For example, when detecting the produced high-energy photons and reconstructing the exclusive missing mass spectra, we can isolate coherent DVCS events from the electron scattering off the entire ^{3}H and ^{3}He nuclei. By measuring the coherent DVCS cross-sections, extraction of the Compton Form Factors (which link to the generalized parton distributions (GPDs) of ^{3}H and ^{3}He nuclei - spin-1/2 particles that contain similar sets of GPDs defined in the nucleons) is possible. Theoretical calculations [61] [61] [62] [63] suggest that the ^{3}He GPDs are dominated by the contribution from the neutron's GPD-E, extremely important for studying the orbital angular momentum of the nucleons. Using ^{3}H as a mirror nucleus

enables us to perform flavor-separation of individual quarks' GPDs in the $A = 3$ system. We can also measure incoherent DVCS, DVCS from individual bound protons or neutrons, to further study the medium modification effect of the GPDs in nuclei that cannot be studied elsewhere.

Such a DVCS measurement can be carried out in parallel with the SIDIS measurement discussed in this proposal without additional experimental configurations or beam-time. In our Tritium-CLAS12 collaboration, we have another group of experts working on preparing an additional new $A = 3$ DVCS proposal, which will run together with the SIDIS measurement and illuminate other potential topics, for example, the Deep Virtual Meson Production (DVMP) with multiple types of final state mesons. We will submit a new proposal to the PAC to study the exclusive reactions in the coming year, and together with this SIDIS proposal, we can form a strong run-group experiment to exclusively study the 3D structure of $A = 3$ nuclei.

References

[1] Or Hen et al. Precision measurements of A=3 nuclei in Hall B, 9 2020.

[2] N. Brambilla et al. QCD and Strongly Coupled Gauge Theories: Challenges and Perspectives. *Eur. Phys. J. C*, 74(10):2981, 2014.

[3] Edward V. Shuryak. Quantum Chromodynamics and the Theory of Superdense Matter. *Phys. Rept.*, 61:71–158, 1980.

[4] J.J. Aubert et al. *Phys. Lett. B*, 123:275, 1983.

[5] D.F. Geesaman, K. Saito, and A.W. Thomas. The Nuclear EMC Effect. *Ann. Rev. Nucl. and Part. Sci.*, 45:337, 1995.

[6] P. R. Norton. *Rep. Prog. Phys.*, 66:1253, 2003.

[7] S. Malace, D. Gaskell, D. W. Higinbotham, and I. C. Cloët. The challenge of the emc effect: Existing data and future directions. *International Journal of Modern Physics E*, 23(08):1430013, 2014.

[8] O. Hen, G. A. Miller, E. Piasetzky, and L. B. Weinstein. Nucleon-Nucleon Correlations, Short-lived Excitations, and the Quarks Within. *Rev. Mod. Phys.*, 89(4):045002, 2017.

[9] J. Gomez et al. Measurement of the a dependence of deep-inelastic electron scattering. *Phys. Rev. D*, 49:4348, 1994.

[10] J. Seely et al. New measurements of the european muon collaboration effect in very light nuclei. *Phys. Rev. Lett.*, 103:202301, 2009.

[11] I. Cloet, W. Bentz, and A. W. Thomas. *Phys. Lett. B*, 642:210, 2006.

[12] A. C. Benvenuti et al. A High Statistics Measurement of the Nucleon Structure Function F(2) (X,Q^2) From Deep Inelastic Muon - Carbon Scattering at High Q^2. *Phys. Lett. B*, 195:91–96, 1987.

[13] D. M. Alde et al. Nuclear dependence of dimuon production at 800-GeV. FNAL-772 experiment. *Phys. Rev. Lett.*, 64:2479–2482, 1990.

[14] L. B. Weinstein, E. Piasetzky, D. W. Higinbotham, J. Gomez, O. Hen, and R. Shneor. Short range correlations and the emc effect. *Phys. Rev. Lett.*, 106(5):052301, Feb 2011.

[15] N. Fomin et al. New measurements of high-momentum nucleons and short-range structures in nuclei. *Phys. Rev. Lett.*, 108:092502, 2012.

[16] O. Hen, E. Piasetzky, and L. B. Weinstein. New data strengthen the connection between short range correlations and the emc effect. *Phys. Rev. C*, 85:047301, Apr 2012.

[17] B. Schmookler et al. Modified structure of protons and neutrons in correlated pairs. *Nature*, 566(7744):354–358, 2019.

[18] J. Arrington, A. Daniel, D. B. Day, N. Fomin, D. Gaskell, and P. Solvignon. Detailed study of the nuclear dependence of the emc effect and short-range correlations. *Phys. Rev. C*, 86:065204, Dec 2012.

[19] E. Piasetzky, M. Sargsian, L. Frankfurt, M. Strikman, and J. W. Watson. Evidence for the strong dominance of proton-neutron correlations in nuclei. *Phys. Rev. Lett.*, 97:162504, 2006.

[20] R. Subedi et al. Probing cold dense nuclear matter. *Science*, 320:1476, 2008.

[21] O. Hen, G. A. Miller, E. Piasetzky, and L. B. Weinstein. Nucleon-Nucleon Correlations, Short-lived Excitations, and the Quarks Within. *Rev. Mod. Phys.*, 89(4):045002, 2017.

[22] M. Duer et al. Direct Observation of Proton-Neutron Short-Range Correlation Dominance in Heavy Nuclei. *Phys. Rev. Lett.*, 122:172502, 2019.

[23] J. Arrington and N. Fomin. Searching for flavor dependence in nuclear quark behavior. *Phys. Rev. Lett.*, 123:042501, 2019.

[24] R. Cruz-Torres et al. Many-body factorization and position–momentum equivalence of nuclear short-range correlations. *Nature Phys.*, 17(3):306–310, 2021.

[25] Jennifer Rittenhouse West. Diquark Formation from Nucleon-Nucleon Interactions I: Nuclear Matter, arXiv:2009.06968, 2021.

[26] Jennifer Rittenhouse West, Stanley J. Brodsky, Guy F. de Teramond, Alfred S. Goldhaber, and Ivan Schmidt. QCD hidden-color hexadiquark in the core of nuclei. *Nucl. Phys. A*, 1007:122134, 2021.

[27] I. C. Cloet, W. Bentz, and A. W. Thomas. Isovector EMC effect explains the NuTeV anomaly. *Phys. Rev. Lett.*, 102:252301, 2009.

[28] I. Cloet, W. Bentz, and A. W. Thomas. *Phys. Rev. Lett*, 109:182301, 2012.

[29] I. Cloet et al. Exposing novel quark and gluon effects in nuclei. *J. Phys., G*, 46:093001, 2019.

[30] I. C. Cloet, Wolfgang Bentz, and Anthony William Thomas. EMC and polarized EMC effects in nuclei. *Phys. Lett.*, B642:210–217, 2006.

[31] D. Adams et al. Measurement of the Nucleon F_2^n/F_2^p Structure Function Ratio by the Jefferson Lab MARATHON Tritium/Helium-3 Deep Inelastic Scattering Experiment. *arXiv:2104.05850*.

[32] C. Cocuzza et al. Isovector EMC effect from global QCD analysis with MARATHON data. *arXiv:2104.06946*.

[33] Ingo Sick and Donal Day. The emc effect of nuclear matter. *Physics Letters B*, 274(1):16 – 20, 1992.

[34] A. Airapetian et al. Quark helicity distributions in the nucleon for up, down, and strange quarks from semi-inclusive deep-inelastic scattering. *Phys. Rev. D*, 71:012003, Jan 2005.

[35] E. P. Segarra et al. Nucleon off-shell structure and the free neutron valence structure from A=3 inclusive electron scattering measurements. 4 2021.

[36] G. G. Petratos et al. MeAsurement of the F_2^n/F_2^p, d/u RAtios and $A = 3$ EMC Effect in Deep Inelastic Electron Scattering Off the Tritium and Helium MirrOr Nuclei. *Jefferson Lab PAC36 Proposal*, 2010.

[37] S. Bueltmann et al. The structure of the free neutron at large x-bjorken, jefferson lab experiment e12-10-102, 2010.

[38] O. Hen et al. Jefferson Lab experiments E12-11-107 and E12-11-003A.

[39] J. Seely et al. New measurements of the european muon collaboration effect in very light nuclei. *Phys. Rev. Lett.*, 103:202301, 2009.

[40] Pía Zurita. Medium modified fragmentation functions with open source xfitter, 2021.

[41] SoLID Collaboration. Precision measurement of parity-violation in deep inelastic scattering over a broad kinematic range (e12-10-007).

[42] CLAS12 Collaboration. Clas12 sidis experiments: E12-06-112, e12-07-107, e12-09-007, e12-09-008, e12-09-009,e12-20-005.

[43] SoLID Collaboration. Sidis measurements with both longitudinally and transversely polarized protons and ^{3}he target (e12-10-006, e12-11-007,e12-11-108,e12-10-006d/e12-11-108b).

[44] EIC User Group. Science requirements and detector concepts for the electron-ion collider (eic yellow report).

[45] M. Anselmino, M. Boglione, J. O. Gonzalez Hernandez, S. Melis, and A. Prokudin. Unpolarised Transverse Momentum Dependent Distribution and Fragmentation Functions from SIDIS Multiplicities. *JHEP*, 04:005, 2014.

[46] Zhong-Bo Kang, Alexei Prokudin, Peng Sun, and Feng Yuan. Extraction of quark transversity distribution and collins fragmentation functions with qcd evolution. *Phys. Rev. D*, 93:014009, Jan 2016.

[47] M. Wakamatsu. Transverse momentum distributions of quarks in the nucleon from the Chiral Quark Soliton Model. *Phys. Rev. D*, 79:094028, 2009.

[48] Hrayr H. Matevosyan, Wolfgang Bentz, Ian C. Cloet, and Anthony W. Thomas. Transverse Momentum Dependent Fragmentation and Quark Distribution Functions from the NJL-jet Model. *Phys. Rev. D*, 85:014021, 2012.

[49] Nematollahi, H., Abolhadi, P., Atashbar, S., Mirjalili, A., and Yazdanpanah, M. M. Polarized parton distribution functions: parametrization and transverse momentum dependence. *Eur. Phys. J. C*, 81(1):18, 2021.

[50] Vincenzo Barone, Stefano Melis, and Alexei Prokudin. The Boer-Mulders effect in unpolarized SIDIS: An Analysis of the COMPASS and HERMES data on the cos 2 phi asymmetry. *Phys. Rev. D*, 81:114026, 2010.

[51] Ralf Seidl. Study of fragmentation function at Belle. *PoS*, DIS2018:154, 2018.

[52] T. Navasardyan et al. The Onset of Quark-Hadron Duality in Pion Electroproduction. *Phys. Rev. Lett.*, 98:022001, 2007.

[53] Jennifer Rittenhouse West, Stanley J. Brodsky, Guy F. de Téramond, and Iván Schmidt. Diffractive dissociation of alpha particles as a test of isophobic short-range correlations inside nuclei. *Phys. Lett. B*, 805:135423, 2020.

[54] A. Airapetian et al. Hadronization in semi-inclusive deep-inelastic scattering on nuclei. *Nucl. Phys. B*, 780:1–27, 2007.

[55] W. Brooks. Quark Propagation Through Cold QCD Matter, Jefferson Lab Proposal E02-104, 2002.

[56] J. Bane. Ph.d thesis the emc effect in a=3 nuclei.

[57] S.A. Kulagin and R. Petti. Global study of nuclear structure functions. *Nuclear Physics A*, 765(1):126 – 187, 2006.

[58] I. Cloet, W. Melnitchouk, N. Sato, J.R. West, and F. Yuan. Private communication.

[59] D. Rimal et al. Measurement of two-photon exchange effect by comparing elastic $e^{\pm}p$ cross sections. *Phys. Rev. C*, 95(6):065201, 2017.

[60] R. Cruz-Torres et al. Probing Few-Body Nuclear Dynamics via ^{3}H and ^{3}He $(e, e'p)$pn Cross-Section Measurements. *Phys. Rev. Lett.*, 124(21):212501, 2020.

[61] S. Scopetta. Conventional nuclear effects on generalized parton distributions of trinucleons. *Phys. Rev. C*, 79:025207, Feb 2009.

[62] M. Rinaldi and S. Scopetta. Extracting generalized neutron parton distributions from ^{3}he data. *Phys. Rev. C*, 87:035208, Mar 2013.

[63] Matteo Rinaldi and Sergio Scopetta. Theoretical description of deeply virtual Compton scattering off ^{3}He. *Few Body Syst.*, 55:861–864, 2014.

[64] D Meekins. Hall A Tritium Target TGT-RPT-17-003. Technical report, Thomas Jefferson National Accelerator Facility, Newport News, 2017.

[65] Andrew J Duncan and Michael J Morgan. Effect of Tritium on Cracking Threshold in 7075 Aluminum. Technical report, Savannah River National Laboratory, 2017.

[66] S.N. Santiesteban, S. Alsalmi, D. Meekins, C. Ayerbe Gayoso, J. Bane, S. Barcus, J. Campbell, J. Castellanos, R. Cruz-Torres, H. Dai, T. Hague, F. Hauenstein, D.W. Higinbotham, R.J. Holt, T. Kutz, S. Li, H. Liu, R.E. McClellan, M. Nycz, D. Nguyen, B. Pandey, V. Pandey, A. Schmidt, T. Su, and Z. Ye. Density changes in low pressure gas targets for electron scattering experiments. *Nuclear Instruments and Methods in Physics Research Section A: Accelerators, Spectrometers, Detectors and Associated Equipment*, 940:351–358, oct 2019.

[67] D. Meekins. TGT-CALC-103-010 Estimated Pressure In Tritium Cell and Permeation Rate. Technical report, Thomas Jefferson National Accelerator Facility, Newport News, Va, 2017.

[68] H. M. HM M. HM Flower. Electron irradiation induced aqueous corrosion of aluminium and magnesium. *Radiation Effects*, 33(3):173–179, 1977.

[69] S. G. Homann. Hotspot health physics codes, version 00, 3 2010.

A Target Design for new SRC Experiment E12-20-005

A new gas target system was proposed for the E12-20-005 measurement [1]. That target system will be suitable for the proposed experiment as well. While a detailed conceptual design is not presented here, we propose that such a system should build on the experiences and lessons learned from the Hall A Tritium Target (HATT) which is described in detail in reference [64]. While this system would be unique, the same rigor that was applied to the Hall A system would also be applied in Hall B. The safety systems and subsystems for the proposed target are necessarily complex and can only be summarized in this proposal. This includes numerous engineered and administrative controls, only some of which are listed below.

- A minimum of three layers of containment and or confinement shall be employed at all times. This includes operations, installation/removal, shipping and handling, and storage.
- The cell shall be constructed in compliance (and indeed in excess of compliance) with JLAB pressure safety requirements, SRTE safety basis requirements, and applicable ASME Codes, namely ASME B31.3 and ASME BPVC VIII D1 and D2. Design safety factors for the cell shall exceed 10. This shall be verified by through destructive testing.
- Strict access controls shall be required for the Hall while the cell is installed. These include specific training, locked badge access to the Hall including truck ramp access, and procedures for entrance/exit of the Hall. These controls are partly to ensure that the Hall will be the third layer of confinement while the cell is installed.
- An extensive review process shall be employed, specifically:
  - Technical and Peer reviews as required my EHSQ 6151 and supplement.
  - Review by Savannah River Tritium Enterprises and DOE-NNSA.
  - Multiple reviews by JLAB and outside Subject Matter Experts (SME) as part of the formal ERR process addressing all aspects of the system.
- Full Failure Mode Effects and Criticality Analysis (FMECA) shall be performed and reviewed by SMEs. All failure modes shall be addressed including complete failure of the containment/confinement system.
- Examinations of materials, completed components, welds, mechanical fabrications, etc. shall be performed by qualified personnel in accordance with approved procedures.
- Inspections verifying all appropriate examinations have been performed and documented by qualified personnel using correct procedures and calibrated/certified equipment.
- Specific training and additional qualifications shall be required for all personnel accessing the Hall and performing any fabrication function.
- A thorough review and site inspection by EHS and Physics Div SMEs ensuring all applicable safety systems are installed and are operating correctly shall be performed.

The proposed system would employ three sealed gas cells filled with $^2H_2$, $^3H_2$, and ^3He. Given the limited space in CLAS12, a motion system is not possible, and the cells would need to be installed separately, marking three distinct run periods. The Hall B tritium target is expected to incorporate the same major components as the Hall A system which are listed below.

- Target Cell
- Exhaust system including stack

- Containment/confinement system including the scattering chamber and Hall B under strict access controls.
- Cryogenic cooling system

Some conceptual design work has been performed and is shown in the subsections below. Rate estimates reported elsewhere in this proposal are based, at least in part, on the thicknesses, materials, and geometries presented in this concept.

A.1 Tritium Containment and Confinement

The primary method for ensuring safe operations with tritium is to establish multi-layer containment and or confinement at all times. The proposed system would rely on a series of engineering and administrative controls to provide at least three layers of tritium confinement and/or containment during all phases of operation. Confinement as defined here would limit a possible tritium release to a controlled region were it would be collected and stacked (exhausted to the environment) in a safe manner. A summary of the three layers of containment/confinement are shown in the table below for each operational condition (configuration).

Configuration	Layer 1	Layer 2	Layer 3
Installation/Removal	Cell	Handling Hut and Scattering Chamber	Hall B
Shipping/Storage	Cell	Inner Containment Vessel	Outer Containment Vessel
Beam Operations	Cell	Scattering Chamber	Hall B

It is important to note that during beam operations, the Hall and scattering chamber must each be considered as one layer of the confinement system. This has implications for the design of the scattering chamber. It also requires that the exhaust system and access controls are designed to ensure that the Hall and chamber can indeed be considered layers of confinement.

A.2 Target Cell

A conceptual model of the cell is shown in Figures 14, 15, and 16. With the exception of the fill valve assembly, the cell is fabricated from ASTM B209 7075-T651 aluminum. This material has many distinct advantages, primarily, being nearly twice the strength and hardness of more common alloys (e.g. 6061). It has also undergone Jefferson Lab sponsored testing at Savannah River National Laboratory confirming suitability for tritium service at our operating conditions [65]. The proposed cell for the Hall B target allows full azimuthal angle acceptance and backward polar angle acceptance, with minimal loss of target length, to 120°. The azimuthal symmetry also greatly simplifies the design of the target cell making it much easier to fabricate than the HATT cell. The target cell is expected to be 12.7 mm in diameter and 25 cm long with a fill pressure of about 200 psi. Thus, the total amount of tritium would be about 1200 Ci. The thickness of the cell wall is 0.4 mm with the exception of the beam entrance and exit which are expected to be 0.25 mm. While these thicknesses are not optimal when considering the physics, they do provide a suitable level of safety both during beam operations and during the filling of the cell off site. Similar sealed gas cells were used in Hall A for the Tritium Family of experiments and performed at $22.5\mu A$ with acceptable density reduction [66]. Filling of the tritium cell is expected to be performed at Savannah River Site where overpressure protection requirements are substantially higher than the fill/operating pressure of the cell.

Hydrogen is known to permeate through most materials. A model was developed for the expected permeation of tritium from the HATT cell [67]. The expected operational loss of tritium from the

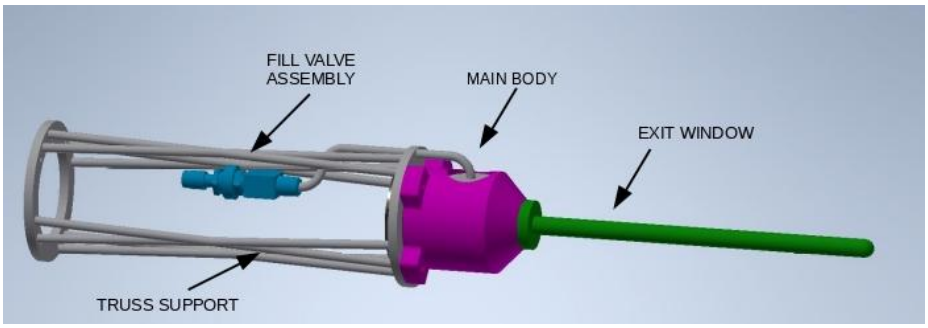

Figure 14: External side view of the conceptual design of the target cell as seen from the beam right side.

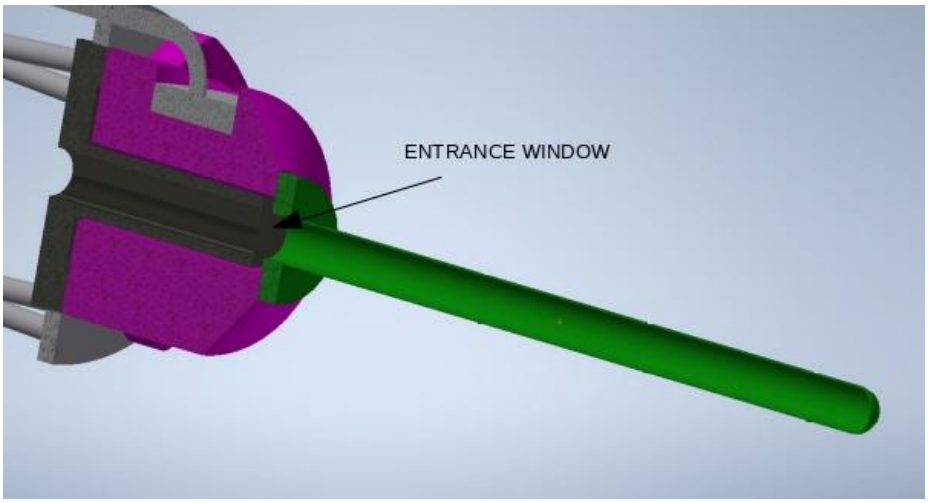

Figure 15: Section view of the conceptual design of the target cell.

cell is less than 0.8 Ci per year due mostly to permeation through the thin cell walls. This is similar to the loss observed in Hall A during operations. This loss, although small, would be collected by the pumping system and stacked.

The temperature of the cell wall should not exceed 170K for extended periods of time. This is a design requirement based on previous studies of hydrogen embrittlement in aluminum with an impinging electron beam [68]. In Hall A, the cooling system was supplied by 15K helium from the ESR. For practical reasons, a dedicated cooling system (similar to that of the Hall D cryogenic target) should be used for a Hall B target. A stand alone pulse-tube refrigerator system such as the CryoMech PT410 with a cold finger would simplify the design and provide operational reliability. The beam current necessary to complete the measurements is much less than $1\mu A$. The heat generated in the cell with this current would be less than 1 W, with the majority being generated in the entrance and exit windows. A thermal model of the cell exit window (the component most affected by the heat load) has been developed assuming following conditions

- Beam current $1\,\mu A$
- Beam spot size of 0.250 mm
- Cold sink operating temperature 40K

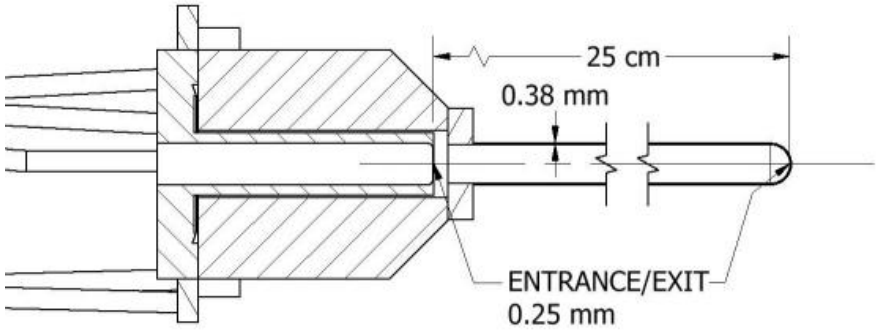

Figure 16: Detail side section view of the target cell with thickness and length. Note that the active region of the cell is 25 mm long.

- Cold finger length 3 m
- Cold finger cross section 1 cm^2
- Model is run in steady state only

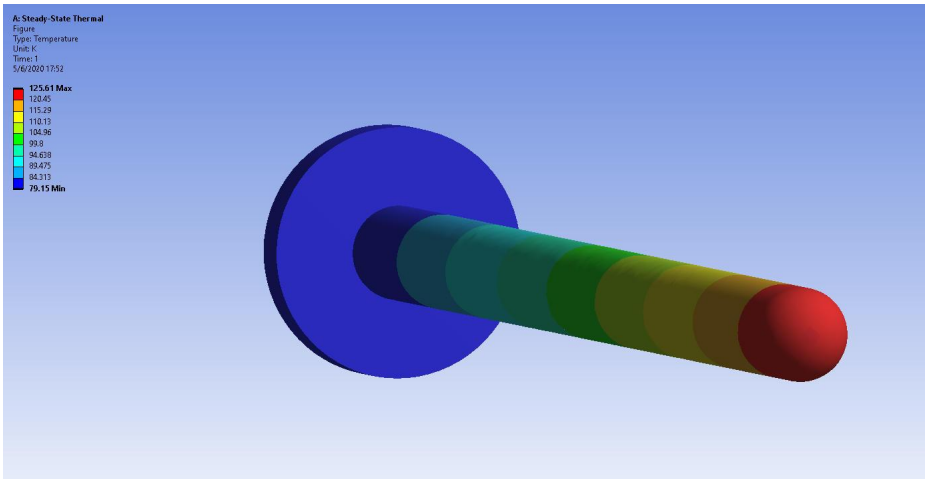

Figure 17: Temperature profile of the aluminum exit window under the conditions listed above. The maximum temperature (red) is 126K and minimum (blue) is 80K

The model was developed using an ANSYS steady state thermal analysis. The results of this simulation are shown in Figures 17 and 18

A.3 Scattering Chamber and Vacuum System

Because the scattering chamber must be a layer of tritium confinement, it cannot be fabricated from materials that are significantly permeable to tritium. Thus, the foam chamber typically used in Hall

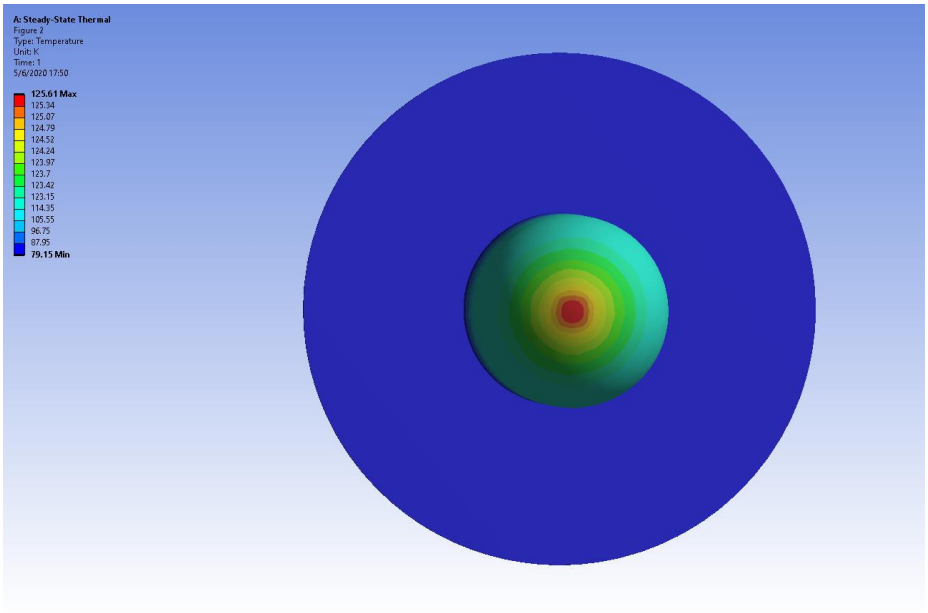

Figure 18: Temperature profile of the exit window tip under the beam conditions listed above. Note that the beam passes through the dark red area in a uniform 0.250 mm spot size and that the temperature scale in this figure has been logarithmically inflated near the tip.

B will have to be replaced. We propose a chamber fabricated from aluminum (ASTM B209 7075-T651) with geometry as shown in Figure 19. In this design, the part of the chamber surrounding the cell is cylindrical with a hemispherical head and has a diameter of 25 mm. Some details of the chamber geometry are shown in Figure 20. Calculations (in compliance with ASME Boiler and Pressure Vessel Code Sec VIII Div 1 and Div 2) show that a wall thickness of 0.4 mm will exceed a safety factor of 2 for buckling from the external pressure. The beam exit of the chamber (tip of the hemisphere) shall be thinned to 0.25 mm. The chamber must also be isolated from the upstream beam line via a 0.2 mm thick beryllium window. Additionally, the chamber volume must be large enough to contain a gas cell failure and still maintain a sub-atmospheric pressure. The vacuum in the chamber would be maintained by a series of mechanical and turbo pumps which would exhaust to the stack.

A.4 Luminosities

It is important to consider that the aluminum walls of the target cell and scattering chamber in the proposed design are relatively much thicker than the nominal Hall B cryotarget configuration. The reasons for this have been discussed in the previous sections. A summary of the assumed thickness and luminosity for the tritium cell, both fluid and metallic components, is shown in Table 3. The fluids in the $^2H_2$ and ^3He cells are expected to have fluid densities of 125% and 150% of the tritium cell. The entrance and exit windows (Al windows) for the cell and chamber have been combined into one thickness.

A.5 Exhaust System and Stack

A dedicated exhaust system and stack shall be constructed to remove tritium from Hall B similar to the system developed for Hall A. Calculations for tritium release resulting from a catastrophic cell failure were performed using HotSpot [69]. This is a DOE approved collection of atmospheric

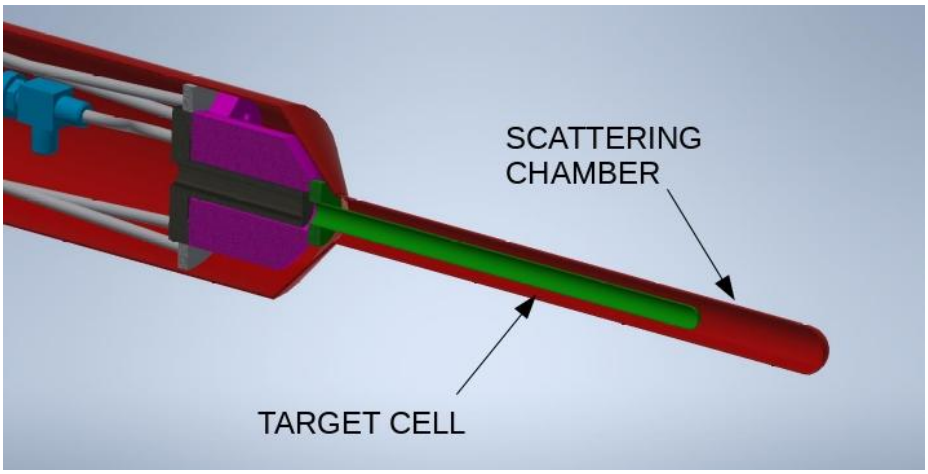

Figure 19: Section view of the target cell/chamber assembly

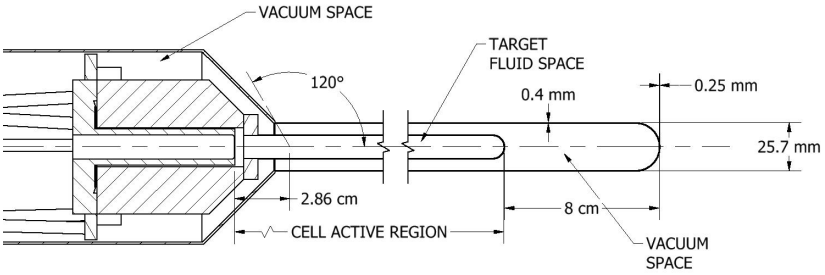

Figure 20: Detail section view cell/chamber assembly with some dimensional detail. Note that for 120° the effective length of the target is shortened by less than 3 cm.

dispersion models which are designed for near-surface releases, short-range (less than 10 km) dispersion, and short-term (less than 24 hours) release durations in unobstructed terrain and simple meteorological conditions. These calculations, summarized in [64], indicate the exhaust stack must be at least 20 m above grade at the site boundary. (Note the the position of the Hall B stack would be less than 15 m from the current Hall A stack.) This ensures that any release will not cause an undue exposure to the public. The exhaust system shall be driven by a fan which pulls air through Hall B (maintaining a slight negative pressure) into the stack via one of the smoke removal ports. Thus, the exhaust system serves two purposes: tritium removal and smoke removal. This system must also stack the exhaust from the vacuum pumps connected to the scattering chamber and downstream beam line. These subsystems are necessary to ensure at least three layers of containment or confinement as discussed previously.

Material	Tritium	Al Windows	Be Window	Total
Length(g/cm^2)	0.085	0.21	0.037	0.33
Luminosity	3.54×10^{34}	8.42×10^{34}	1.54×10^{34}	1.35×10^{35}

Table 3: Assumed density and luminosity for each component. Note that the maximum luminosity of CLAS12 is 1.35×10^{35} nucleon/cm^2/s

A.6 Transportation and Storage

The HATT cell was filled at Savannah River Site and shipped to Jefferson Lab in the Bulk Tritium Shipping Package (BTSP) as a miscellaneous tritium vessel (MTV). The same mechanism is expected to be employed for filling and shipping a similar cell for the Hall B target. An expert team from SRS traveled to Jefferson Lab to assist in the unpackaging and packaging of the cell to and from the BTSP. The Hall B tritium cell would be filled and transported in the same manner. The storage system employed in Hall A can also be used in Hall B. This system allowed the target cell to be removed from the beam line for longer term storage (up to a few months) during accelerator down periods. It also simplifies packaging and unpackaging operations associated with shipment of the cell.